Alma Mater Studiorum · Università di Bologna

Scuola di Scienze

Corso di Laurea Magistrale in Fisica

Quantum Biology. Simulazioni di trasferimento di energia in una struttura dimerica

Relatore:

Prof.sa Beatrice Fraboni

Correlatore:

Dott. Javier Prior Arce

Presentata da:

Adriano Macarone Palmieri

Sessione II

Anno Accademico 2013/2014

Indice

1 Introduction/Abstract **5**

1.1 Abstract 5

1.2 Introduction 6

1.3 Biological Introduction 7

1.3.1 Electronic energy transfer in Photosyntetic complex 11

1.3.2 Phonon-assisted electron tunneling & olfaction 12

1.3.3 Magneto reception in birds 13

2 Dynamical Simulation of 1-D Quantum Many body Systems **15**

2.1 Introduction 15

2.2 1D Quantum Systems 16

2.2.1 Definition 16

2.2.2 Basic Properties of 1D quantum systems 17

2.2.3 Schmidt decomposition 17

2.3 Matrix Product Representation 19

2.3.1 Schmidt decomposition and canonical form 20

2.4 Calculations with MPS 22

2.4.1 Density matrices 22

2.4.2 Two-sites gates 23

3 Time Evolving Block Decimation **27**

3.0.3 Suzuki-Trotter sweeps 28

3.1 Errors In TEBD 29

3.1.1 Trotter error 29
3.1.2 Truncation error 30

4 Mapping between system-reservoir & semi-infinite discrete chains 33
4.1 Introduction 33
4.1.1 System Reservoir structure 35
4.1.2 Applications 38

5 Photosynthesis networks transport 43
5.1 The phonon antenna mechanism 43
5.1.1 Non equilibrium long lived coherences 45
5.1.2 Last overview on EET principles 45
5.2 TEBD simulation for Dimeric system 47
5.2.1 Introduction 47
5.2.2 Model parameters 48
5.2.3 The Adolf-Rengel optical spectral 48
5.2.4 the recoherence and the fundamental role of non-equilibrium vibrational structure 51
5.2.5 the coupling with environment 52
5.2.6 Additional random noise 53
5.2.7 entanglement Measures: Von Newman entropy 57
5.2.8 The Double Environment 64

6 Conclusion 69

Capitolo 1

Introduction/Abstract

1.1 Abstract

La quantum biology (QB) è un campo di ricerca emergente che cerca di affrontare fenomeni quantistici non triviali all'interno dei contesti biologici dotandosi di dati sperimentali di esplorazioni teoriche e tecniche numeriche. I sistemi biologici sono per definizione sistemi aperti, caldi,umidi e rumorosi, e queste condizioni sono per loro imprenscindibili; si pensa sia un sistema soggetto ad una veloce decoerenza che sopprime ogni dinamica quantistica controllata. La QB, tramite i principi di noise assisted transport e di antenna fononica sostiene che la presenza di un adeguato livello di rumore ambientale aumenti l'efficienza di un network di trasporto,inoltre se all'interno dello spettro ambientale vi sono specifici modi vibrazionali persistenti si hanno effetti di risonanza che rigenerano la coerenza quantistica. L'interazione ambiente-sistema è di tipo non Markoviano,non perturbativo e di forte non equilibrio, ed il rumore non è trattato come tradizionale rumore bianco. La tecnica numerica che per prima ha predetto la rigenerazione della coerenza all'interno di questi network proteici è stato il TEBD, Time Evolving Block Decimation, uno schema numerico che permette di simulare sistemi 1-D a molti corpi, caratterizzati da interazioni di primi vicini e leggermente entangled. Tramite gli algoritmi numerici di Orthopol l'hamiltoniana spin-bosone viene proiettata su una catena discreta 1-D, tenendo conto degli effetti di interazione ambiente-sistema contenuti nello spettro(il quale determina la dinamica del sistema).Infine si esegue l'evoluzione dello stato.

1.2 Introduction

The recently born approach towards some biological effects and their new type of description it's demonstrating to be quite challenging both theoretically and experimentally. Recently the numerical approach of TEBD (Time Evolving Block Decimation), inherited from quantum information, has assisted the idea (and some experimental data) that typical quantum effects like the presence of coherence and local entanglement play an important, even if partly still unclear, role in some biological effects like the EET. Moreover the theoretical and numerical challenge to interpret and modeling these phenomena, the great difficulties given from the experimental data and their complex interpretation, at the light of our current knowledges is still quite great. To begin with, biological systems are, almost by definition, open systems, as they need to be continuously supplied with energy to maintain the out of equilibrium state that life represents. Open systems, however, especially warm, wet and noisy biological systems, are subject to environmental fluctuations that are usually expected to result in fast decoherence and, as a result, the suppression of well controlled quantum dynamics. Thus quantum phenomena may at first sight seem unlikely to play a significant role in biology. These quantum phenomena are not merely a by-product of the underlying quantum nature of chemical bonds but are actually exploited by biological systems to enhance performance and achieve novel functionalities. The extreme consequence of the basic principle of phonon antenna have been found to underlie the fruitful interplay between vibrational environments and coherent quantum dynamics, which will provide an understanding why optimal transport performance in proteic complex can arise at intermediate noise levels.Let's take two closely spaced energy levels are separated from a third level to which excitations should be delivered. They are subject to dephasing noise from an environment with a finite bandwidth that exhibits a maximum. A coherent interaction between the upper two energy levels leads to dressed states $|\pm\rangle$ with an energy splitting which, if matched to the maximum of the environment spectral density, will optimize transport from the upper to the lower level. As will be shown in the data chapter, the presence of sharp resonant peak into the spectra that, as in

the case of EET , if it matches enough the difference in energy between two different exciton produce a further tuning effect that will give raise to the reborn of the coherence in the system. Theoretically the most simple model is the Spin-Boson Model (SBM) one of the simplest non-trivial models of open-system dynamics. This model describes a single two-level system (TLS) coupled linearly to the coordinates of an environment consisting of a continuum of harmonic oscillators and despite its simplicity, this model shows a rich array of non-Markovian dynamical phenomena that for picoseconds time become of relevant importance. This non Markovian backward effects of interaction due to the system environment coupling are the key element of the lasting of coherence into the system. Mapping the spin-boson model exactly onto a 1D system permits the deployment of the time-adaptive density matrix where renormalization group (t-DMRG), to which TEBD belongs, technique to integrate the time evolution of the full system-environment dynamics efficiently

1.3 Biological Introduction

Following early speculations concerning the potential role of quantum physics in biology, recent progress in science and technology has led to the rapid emergence of a new direction of research whose aim is the experimental and theoretical exploration of quantum effects in biology (see [1][2]) which are taking place on length and timescales that allow quantum dynamics and environmental fluctuations to enter an intricate and fruitful interplay. To begin with, biological systems are, almost by definition, open systems, as they need to be continuously supplied with energy to maintain the out of equilibrium state that life represents. Open systems, however, especially warm, wet and noisy biological systems, are subject to environmental fluctuations that are usually expected to result in fast decoherence and, as a result, the suppression of well controlled quantum dynamics. Thus quantum phenomena may at first sight seem unlikely to play a significant role in biology. There are arguments however to counter this pessimistic view. At the level of molecular complexes and proteins, processes that are of fundamental importance for biological function can

be very fast (taking place within picoseconds) and well localised (extending across a few nanometers, the size of proteins) and may therefore exhibit quantum phenomena before the environment has had an opportunity to destroy them. Furthermore, early work in quantum information science, for example, has shown that thermal noise in stationary non-equilibrium systems may in fact support the existence of quantum coherence and entanglement [3]. Hence the possible existence of significant quantum dynamics is not only a question of sufficiently short length and time scales but may also depend on a constructive interplay between a quantum dynamical system and its environment such that quantum correlations are not simply washed out or suppressed but may in fact be enhanced or regenerated by the interaction with the environment. These arguments suggest that quantum effects in biology are possible at the right length- and time scales. We do expect however that in the course of evolution Nature will have learnt to make use of quantum phenomena only if these enable or make more efficient a useful biological function that provides an evolutionary advantage. It is indeed well established from a quantum information perspective that pure quantum dynamics of multi-component systems can provide qualitative performance improvements over classical systems for example where transport is concerned. This provides further support for the expectation that nature has developed non-trivial quantum phenomena in the dynamics of biological systems, possibly supported by their environment whose presence and influence is unavoidable. These quantum phenomena are not merely a by-product of the underlying quantum nature of chemical bonds but are actually exploited by biological systems to enhance performance and achieve novel functionalities. The clear demonstration that Nature makes use of quantum effects would bring about the necessity for a significant change of thinking for biologists as they would be required to grasp quantum concepts in order to understand some fundamental biological processes. As above stated when the biological system seems to take advantage from local quantum properties and are able to handle them despite the presence of a surrounding which, in truth, as we'll be better explained in chapter 4, can become a resource for the permanence and reborn of quantum properties, instead of the cause of the death of these physical elements. Being so, we can start to think to apply technique

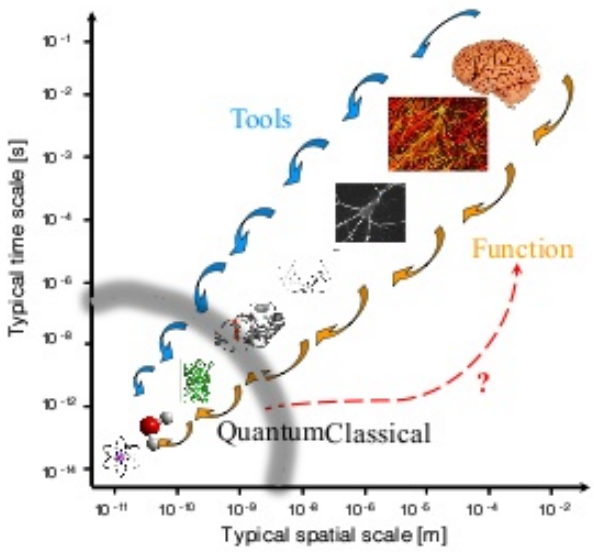

Figura 1.1: dimensions & correlated biological phenomena and complexity

typical of the many body system into these kind of contests, but taking in mind that the biological system can be treated uniquely as Open Quantum System and taking in account of the very fast (picosecond time scale) time setting of these transient phenomena,the perturbative approximation cannot suits our necessities.

Open Quantum Systems–Thanks to the insights of quantum physics some unresolved biological phenomena today can be deal with a new approach whereas the old classical interpretations have seemed so far to fail. The energy transport mechanism of clorosomes or into the reaction center of the leafs systems will be developed in the next chapter (see chapter 4) , but today the quantum approach is trying to shed light also onto other different biological phenomena. Needless to say the key component supporting this interpretation is the presence of a environment composed of vibration or spins that can be handled by the system in order to take advantage in sustaining it's quantum properties.Differently from the thermal fluctuations that it's exploited from classical systems in order to overcome potential barrier (a mechanism present in protein folding e.g.) the benefits of environment onto quantum system is less evident and experimentally tasking to explore.

/Structured active Environment]Structured active Environment

As repetitively claimed the environment is not a passive element and in biological contest possess a well define,organized structure.These kinds of environment are not a simple source of white noise and cannot be represented as a small perturbation of any dynamics. All the informations of the environment effect are encoded inside its spectra.The environmental spectral densities (e.g. see chapter 5) describing their interaction with the system tend to display two principal structures:

1. a broad smooth back- ground which has a short memory time and interacts with the system mainly through its fluctuations, i.e. causing noise,

2. sharp defined features corresponding to long-lived vibrational motion

the latter ones can lead to quasi-coherent dynamical non-equilibrium exchanges between system and environment. The first smooth vibrational component of the environment is due to the protein environment and noise processes caused by the

solvents,while the sharp features originate from long lived vibration belonging to molecules inside the protein scaffold. This reachness leads to a non-Markovian and being the environment neither too much nor to weakly coupled compared to the intra-systems dynamics, the total dynamics is also a non-perturbative one. Moreover we must stress a fundamental concept: biological system can survive only continuously managing an out-of-equilibrium state.

1.3.1 Electronic energy transfer in Photosyntetic complex

In physical terms an organised structured like that of the well studied FMO antenna complex is no more than a transport network assigned to the convey of electronic excitations (excitons) , that is composed of a set of highly absorptive entities such bacteriochlorophyll molecules each of which may support an electronic excitation (a Frenkel exciton). The protein scaffold role is to display them into the space into a specific geometry,somebody has also argued that the protein scaffold may give a further help to the transport ability of the network with little variations in the inter-antenna distance and so modifying the dipolar strength between antennas in order to improve the tuning between them. The full Hamiltonian describing the exciton- vibrational interaction as well as the exciton-exciton interaction is given by $H = H_{ex} + H_I + H_B$ where

$$H_{ex} = \sum_{n=1}^{N} E_n |n\rangle\langle n| + \frac{1}{2}\sum_{m\neq n}(|m\rangle\langle n| + h.c.) \tag{1.1}$$

$$H_B = \sum_{i,k} \hbar\omega_k a_{ik}^{\dagger} a_{ik} \tag{1.2}$$

$$H_I = \frac{1}{2}\sum_{n}(\sum_{k} \sqrt{S_{nk}}\omega_k (a_{nk} + a_{nk^{\dagger}})|n\rangle\langle n| + h.c.) \tag{1.3}$$

with $|n\rangle$ the excitation on site n,J_{mn} the dipolar interaction between excitations on different sites, $a_{nk}, a_{nk}^{\dagger}$ the bosonic destruction and creation operators for k^{th} independent vibrational mode coupled to site n. In the end S_{nk} is the Huang-Rhys factor which determined the strength coupling between exciton and vibration mode.

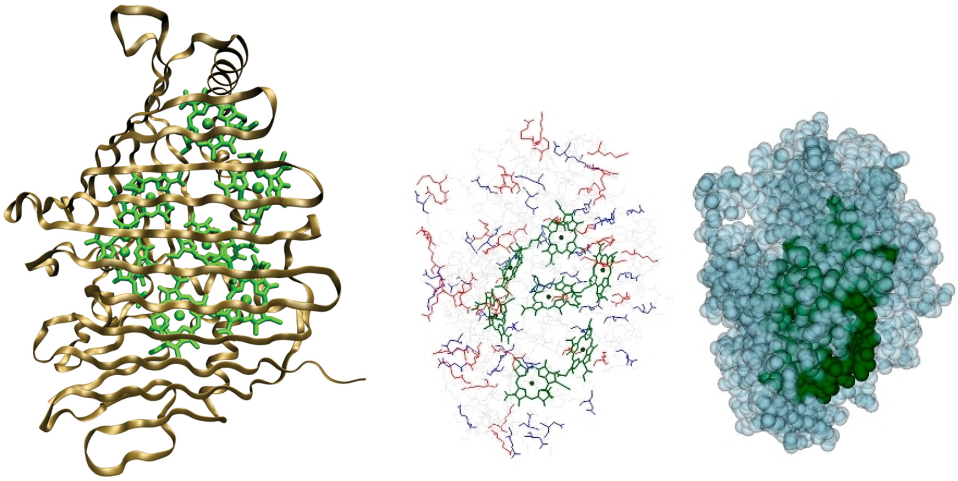

Figura 1.2: Two typical pictorial representation of the Fenna-Matthew-Olson complex.The clorophilla antenna are enveloped inside a structured ,complex, environmental scaffold (here represented with a circular alpha sheet) that sustain the structure of the monomer.

1.3.2 Phonon-assisted electron tunneling & olfaction

Despite considerable progress concerning the under- standing of the structure of olfactory receptors that involved in the early stages of the olfactory process, the detailed mechanisms by which we are able to discriminate between the vast number of odorants are not yet fully understood . This is emphasized by the fact that for nearly 100 years researchers have striven, with limited success, to identify principles that allow for the prediction of smell. The standard idea behind the principles governing the olfactory receptors is the lock-and-key principles, a standard typical approach used also for cellular communication and membrana functions. For many receptors, especially those binding only a very specific molecule, this appears to be a useful and valid principle. Therefore it seems natural to adopt the very same principle also for olfactory receptors. There are at least 100000 odorants but far fewer olfactory receptors – several hundreds in humans, so that there is not a specific receptor for each single odorant. The ability to differentiate such a large number of odorants would thus require that each odorants may bind to a variety of receptors. This would give rise to a vast number of distinct binding patterns and the subsequent

sensation of smell, nonetheless an clear explication hasn't been experimentally founded yet. Moreover has been noticed in recent experiments that Drosophila flies are capable of discriminating between molecules in their hydrogenated and their deuterated form and, importantly, are able to generalize from deuterated molecules to other molecules that exhibit a vibrational modes similar in frequency to the Carbon-Deuterium stretch mode. These observations sustain the alternative theory based on the physical-vibrational properties of the molecules rather then the standard chemical lock-and key mechanism. The physical mechanism besides the olfactory phenomena should be, as proposed by Luca Turin, the inelastic electron tunneling spectroscopy, which allows to recognize the vibrational spectra of a molecula. In the new perspective of noise assisted quantum effects the are the environmental phonon who supported the the inelastic electron tunneling; there is on the one hand the tunneling process of a massive particle, here the electron, and on the other hand the fact that a vibrational mode, that is a quantized harmonic oscillator, can only take up energy in discrete quanta proportional to the relevant vibrational frequency ω_{odor}. It is the second aspect that makes it possible for this process to discriminate effectively between different vibrational modes and thus between the vibrational fingerprints of different molecules.

1.3.3 Magneto reception in birds

Despitethe navigation and orientation ability of lot of mammals,birds reptiles and amphibians is well documented, the mechanism behind this magneto sense of lot of creatures it actually unclear. Recently behavioral experiments with birds such as the Euro- pean robin to study avian magneto-reception have led to the observation that the process of avian magneto- reception depends on the wavelength of the ambient light and can be disrupted by very weak external oscillating magnetic fields. These combined with independent experiments of magnetic field effects on radical pair reaction at a earth magnetic fields provides evidences that support the idea that the chemical compass (which is composed free radicals) may be involved in magneto reception. A donor-acceptor pair is initially in its electronic ground state

characterized by a paired electron in a singlet state. Absorption of a photon induces an electron transfer of a single electron from the donor to the acceptor thus creating a radical pair, that is, two molecules with an unpaired electron each. For simplicity we assume that the electronic spin state remains unaffected in this step so that the electrons remain in a singlet state. At this stage no magnetic field sensitivity can be expected as the spin singlet state is rotationally symmetric and hence insensitive to the orientation and magnitude of the external magnetic field. To break the symmetry is the nuclear spin environment of the donor and acceptor moleculas. Due to the distance dependence of the dipolar interaction between electron and nuclear spin the unpaired electrons on donor and acceptor see dominantly uncorrelated interactions which induce symmetry- breaking transitions from the singlet to the triplet manifold.

Capitolo 2

Dynamical Simulation of 1-D Quantum Many body Systems

2.1 Introduction

Biological systems are not so strictly bounded systems, they best suite the definition of *slightly* entangled systems, but even if they're not a standard strongly-correlated systems as the usual ones utilized in condensed matter physics (e.g. Bose-einstein condensate) as demonstrated by Vidal into they're works it's always possible to perform a classical simulation of the evolution of the quantum state that described these type of states if the computational cost it's not exponential ; so some specific quantum evolutions can be efficiently simulated by a classical computer , and therefore cannot yield an exponential computational speed-up. TEBD makes use of a classical computer, pure-state quantum dynamics of n entangled qubits, whenever only a *restricted* amount of entanglement is present in the system. Consider, a pure state $|\Phi\rangle \in \mathcal{H}_2^{\otimes n}$ of an n-qubit system. Let A denote a subset of the n qubits and B the rest of them. The Schmidt decomposition (SD) of $|\Phi\rangle$ with respect to the partition A:B reads

$$|\Psi\rangle = \sum_{\alpha=1}^{\chi_A} \lambda_\alpha |\Phi_\alpha^{[A]}\rangle \otimes |\Phi_\alpha^{[B]}\rangle \tag{2.1}$$

where the vector $|\Phi_\alpha^{[A]}\rangle$, $|\Phi_\alpha^{[B]}\rangle$ is an eigenvector with eigenvalue $|\lambda_\alpha\rangle$>0 of the reduced density matrix $\rho^{[A]}$, $\rho^{[B]}$ whereas the coefficient λ_α follows from the relation $\langle\Phi_\alpha^{[A]}|\Psi\rangle = \lambda_\alpha|\Phi_\alpha^{[B]}$. The Schmidt rank χ_A is a natural measure of the entanglement between the qubits in A and those in B. Accordingly, we quantify the entanglement of state $|\Psi\rangle$ by χ

$$\chi \equiv \max_A \chi_A \tag{2.2}$$

that is, by the maximal Schmidt rank over all possible bi-partite splittings A:B of the n qubits. We shall say that $|Psi\rangle$ is only slighlty entangled if χ is small. In particular, here we are interested in sequences of states $|\Psi_n\rangle$ of an increasing number n of qubits (corresponding, say, to quantum computations with increasingly large inputs). In such a context we consider χ to be small if it grows at most polynomially with n, $\chi_n = poly(n)$. If through a pure-state quantum computation χ_n is upper bounded by poly(n), then the computation can be classically simulated with poly(n) memory space and computational time, and so reproducible

2.2 1D Quantum systems

2.2.1 Definition

To begin we consider a quantum system composed of M subsystems (or sites) each with an identical local finite d-dimensional Hilbert space $\mathcal{H}_d$ spanned by states $|j\rangle$ The full state space of this system $\mathcal{H} = \mathcal{H}^{\otimes M_d}$is then spanned by the product basis of these local states $|J_{[1,M]}\rangle = |j_1\rangle|j_2\rangle\otimes\cdots|j_M\rangle$ and has dimension $D = d$ which grows exponentially with$M$. An arbitrary state $|\Psi\rangle$ of the system can be expanded in this basis as

$$|\Psi\rangle = \sum_{|j_{[1,M]}\rangle} c_{j_1,j_2\cdots j_M}|J_{[1,M]}\rangle \tag{2.3}$$

with D complex amplitudes $c_{j_1,j_2\cdots j_M}$. While we have imposed a sequential labelling to the subsystems we have not yet made any real constraint on the dimension of the system. Indeed, the actual geometry of the system is only truly revealed by the range and pattern (with respect to the labelling) of interactions between the

underlying subsystems as determined by the Hamiltonian1 of the system. Thus, to restrict our considerations to a genuine 1D quantum system the Hamiltonian $\hat{H}$ governing the system must have short-ranged interactions only.

2.2.2 Basic Properties of 1D quantum systems

The knowledge of how entanglement is distributed within a 1D system permits a parametrisation of low-lying excitation for 1D quantum system[8]. We consider the 1D quantum Ising model with a transverse magnetic field

$$\hat{H}_{Ising} = -J\Big(\sum_{i=1}^{M-1}\sigma_i^x\sigma_{i+1}^x + g\sum_{i=1}^{M}\sigma_i^z\Big) \tag{2.4}$$

since it is exactly solvable. We 'll consider two important properties of the ground state. Firstly, the spin-spin correlations as a function of the distance between the spins l which are of the form

$$C_l^{ab} = \langle\sigma_i^a\sigma_{i+l}^b\rangle - \langle\sigma_i^a\rangle\langle\sigma_{i+l}^b\rangle \tag{2.5}$$

Since correlation functions C_l^{ab} vanish for all product spin states a change in their behaviour is a signature of a corresponding change in the structure of entanglement in the ground state. The second relevant property is the entanglement entropy S_L of a contiguous block of L spins, which is calculated from the block's reduced density matrix $\rho_L = tr_{M-L}(|\Psi_{gs}\rangle\langle\Psi_{gl}|)$ via the von-Neumann entropy

$$S_L = -tr\Big(\rho_L log_2\rho_L\Big) \tag{2.6}$$

and directly measures the amount of entanglement between the block and the rest of the chain.

2.2.3 Schmidt decomposition

The essential mathematical tool we use to build a more efficient formulation is the Schmidt decomposition. Starting from an arbitrary state $|\Psi\rangle$ in the Hilbert space H of an M-site system, we begin by bipartitioning this system into two subsystems

A and B which are composed of some subset of m and $M-m$ sites respectively. By using some orthonormal basis $|i_A\rangle$ spanning the d^m-dimensional Hilbert space H_A and similarly $|j_B\rangle$spanning the d^{M-m} dimensional Hilbert space H_B this arbitrary state can be expressed as

$$|\Psi\rangle = \sum_{i=1}^{d^m}\sum_{j=1}^{d^{M-m}} C_{ij}|i_A\rangle \otimes |j_B\rangle \tag{2.7}$$

The amplitudes C_{ij} of this expansion can then be interpreted as the elements of a $(d^m \times d^{M-m})$ matrix C. We then perform a standard operation of linear algebra, called the singular-value-decomposition (SVD), which breaks C up into the product $C = UDV$, where U and V are $(d^m \times d^m)$and $(d^{M-m} \times d^{M-m})$unitary matrices and D is a $(d^m \times d^{M-m})$diagonal matrix whose elements are real and non-negative . We denote the diagonal elements of D as $\lambda_\alpha = D_{\alpha\alpha}$, and the number of non-zero λ_α's as χ. This operation then brings the expansion into the form of a Schmidt decomposition as

$$\begin{aligned} |\Psi\rangle &= \sum_{\alpha=1}^{\chi}\lambda_\alpha\Big(\sum_{i=1}^{d^m} U_{i\alpha}|i\rangle_A\Big)\otimes\Big(\sum_{j=1}^{d^{M-m}} V_{\alpha j}|j\rangle_B\Big) \\ &= \sum_{\alpha=1}^{\chi}\lambda_\alpha|\phi_\alpha^{[A]}\rangle\otimes|\phi_\alpha^{[B]}\rangle \end{aligned} \tag{2.8}$$

Since the unitary matrices U and V act solely on the corresponding subspaces, H_A and H_B, respectively, they have been used to construct the orthonormal bases, called Schmidt states, $\{|\phi_\alpha^{[A]}\rangle\}$ and $\{|\phi_\alpha^{[A]}\}$which span χ-dimensional subspaces of H_A and H_B respectively. The diagonal elements λ_α are called the Schmidt coefficients which we take from now on as being arranged in descending order so $\lambda_\alpha > \lambda_\alpha + 1$ and satisfy $\sum_\alpha \lambda_\alpha^2 = 1$, while χ is called the Schmidt rank. The reduced density matrices for the two subsystems $\rho_A = tr_B(|\Psi\rangle\langle\Psi|)$and $\rho_B = tr_A(|\Psi\rangle\langle\Psi|)$ then follow from the Schmidt decomposition as

$$\rho_A = \sum_{\alpha=1}^{\chi}\lambda_\alpha^2|\phi_\alpha^{[A]}\rangle\langle\phi_\alpha^{[A]}| \quad ;\rho_B = \sum_{\alpha=1}^{\chi}\lambda_\alpha^2|\phi_\alpha^{[B]}\rangle\langle\phi_\alpha^{[B]}| \tag{2.9}$$

which immediately demonstrates that both ρ_A and ρ_B are diagonal in their respective Schmidt basis and have identical spectra. Important physical quantities follow from the nature of the spectrum $\{\lambda_\alpha^2\}$. In particular it allows entanglement between the two subsystems to be measured via the entropy $S_{[A|B]}$, introduced earlier as S_L, which is computed via the Shannon entropy of spectrum

$$S_{[A|B]} \quad = \quad -\sum_{\alpha=1}^{\chi} \lambda_\alpha^2 \log_2 \lambda_\alpha^2 \tag{2.10}$$

Thus, with the total system in a pure state, entanglement between the two subsystems appears as entropy in the resulting reduced density matrices.

2.3 Matrix Product Representation

The ground states of 1D systems have a several unique properties, so we now come to the question of how to exploit these. The approach w will pursue is based on parameterising the state in the form

$$|\Psi\rangle = \sum_{J_{[1,M]}} f\big(A^{[1]j_1} A^{[2]j_2} \cdots A^{[M]j_M}\big)|J_{[1,M]}\rangle \tag{2.11}$$

where $A^{[M]j_M}$ are a set of d complex matrices of dimension $(\chi_{m-1} \times \chi_m)$ labelled by the physical index j_m. Each site m of the system therefore has a matrix assigned to it dependent on which physical basis state$|j_m\rangle$ it is in. The full set of amplitudes $c_{j_1 j_2 \cdots j_M}$ for the state are then encoded into specific products of such matrices and extracted by the function $f(\cdot)$ which maps $(\chi_0 \times \chi_M)$ matrices to scalars. For this reason Eq. (2.11) is called a matrix product representation.The exact form of the function $f(\cdot)$ depends on the boundary conditions. In the case of periodic boundary conditions (PBC) the matrix product representation of a state is

$$|\Psi\rangle = \sum_{J_{[1,M]}} tr\big(A^{[1]j_1} A^{[2]j_2} \cdots A^{[M]j_M}\big)|J_{[1,M]}\rangle \tag{2.12}$$

where the function f(·) is a conventional matrix trace. For open boundary conditions (OBC) the expansion is

$$|\Psi\rangle = \sum_{J_{[1,M]}} \langle \Phi_0 | A^{[1]j_1} A^{[2]j_2} \cdots A^{[M]j_M} | \Phi_M \rangle | J_{[1,M]} \rangle \tag{2.13}$$

where $|\Phi_0\rangle$ and $|\Phi_M\rangle$ [1]are boundary states in the vector spaces $\mathbb{C}^{\chi_0}$ and $\mathbb{C}^{\chi_M}$, respectively. In this case the function $f(\cdot)$ is then equivalent to the scalar-product with these boundary states. Will make use of this properties.

2.3.1 Schmidt decomposition and canonical forms

Till now we have made no constraints on the form of the matrices $A^{[m]j_m}$. This not only makes this description difficult to interpret, it also makes them harder to handle numerically, but using the insertion of the identity (a gauge freedom) of any non-singular square $(\chi^m \times \chi^m)$ matrix X along with its inverseX^{-1} into the matrix product since$A^{[m]j_m} A^{[m+1]j_{m+1}} = (A^{[m]j_m} X^{-1})(X A^{[m+1]j_{m+1}})$ we can solve this lack. To begin we consider a system with OBC and split it after site k into two contiguous blocks $L = 1, \cdots, k$and $R = k+1, \cdots, M$. Using the gauge freedom we redefine the matrix $A^{[k]j_k}$ as $A^{[k]j_k} \to A^{[k]j_k} D^{-1}$ where D is a diagonal $(\chi_k \times \chi_k)$ matrix with real elements λ_{α_k} , and correspondingly introduce it into the product as

$$\prod_{m=1}^{M} A^{[m]j_m} \to \Big(\prod_{m=1}^{k} A^{[m]j_m} \Big) D \Big(\prod_{m'=k+1}^{M} A^{[m']j'_m} \Big) \tag{2.14}$$

By inserting the resolution of the identity $\sum_{\alpha_k} |\alpha_k\rangle\langle\alpha_k|$ for the vector spaces $\mathbb{C}^{\chi\neg}$, on both sides of the diagonal matrix D the matrix product representation of $|\Psi\rangle$ can then be readily split up into the form

$$|\Psi\rangle \quad = \quad \sum_{alpha=1}^{\chi_k} \lambda_{\alpha_k} |\phi^{[L]}_{\alpha_k}\rangle |\phi^{[R]}_{\alpha_k}\rangle \tag{2.15}$$

[1]Note that for numerical calculation we can set $\chi_0 = 1$ and $\chi_M = 1$ for convenience

where the states of the blocks R and L are

$$|\phi^{[L]}_{\alpha_k}\rangle = \sum_{J_{[1,k]}} \langle \Phi_0|A^{[1]j_1}A^{[2]j_2}\cdots A^{[k]j_k}|\alpha_k\rangle|J_{[1,k]}\rangle \tag{2.16}$$

$$|\phi^{[R]}_{\alpha_k}\rangle = \sum_{J_{[k+1,M]}} \langle \alpha_k|A^{[k+1]j_{k+1}}\cdots A^{[M]j_M}|\Phi_M\rangle|J_{[k+1,M]}\rangle \tag{2.17}$$

The corresponding scalar-products of these block states are

$$\begin{aligned}\langle\phi^{[L]}_{\alpha_k}|\phi^{[L]}_{\alpha_k}\rangle &= \sum_{J_{[1,k]}} \langle \alpha_k|(A^{[k]j_k})^\dagger\cdots(A^{[1]j_1})^\dagger|\alpha_k\rangle\langle\Phi_0|A^{[1]j_1}\cdots A^{[k]j_k}|\beta_k\rangle \\ \langle\phi^{[R]}_{\alpha_k}|\phi^{[R]}_{\alpha_k}\rangle &= \sum_{J_{[k+1,M]}} \langle \Phi_M|(A^{[M]j_M})^\dagger\cdots(A^{[k+1]j_{k+1}})^\dagger|\alpha_k\rangle\langle\beta_k|A^{[k+1]j_{k+1}}\cdots A^{[M]j_M}|\Phi_M\rangle\end{aligned}$$

The splitting of the state introduce another question : the right and left handedness of the matrixes of our state. we introduce the notation $A_\leftarrow$ and $A_\rightarrow$ to signify when an A matrix obeys the corresponding left or righthanded orthonormality constraint. The importance of distinguishing them will be clear in next chapters (especially for handling numerical errors). For the boundary we impose

$$\sum_{j_1=1}^{d}(A^{[1]j_1}_\leftarrow)^\dagger|\Phi_0\rangle\langle\Phi_0|A^{[1]j_1}_\leftarrow = \mathbf{1} \quad \text{lefthanded} \tag{2.18}$$

$$\sum_{j_M=1}^{d} A^{[M]j_M}_\rightarrow|\Phi_M\rangle\langle\phi_M|(A^{[M]j_M}_\rightarrow)^\dagger = \mathbf{1} \quad \text{righthanded} \tag{2.19}$$

To ensure ourseleves Eq. (2.15) to be a Schmidt decomposition of $|\Psi\rangle$ we impose to the A matrices of the left ($[L]$) and right ($[R]$)side to obey one of the following constraints.

$$\sum_{j_1=1}^{d}(A^{[1]j_1}_\leftarrow)^\dagger A^{[1]j_1}_\leftarrow = \mathbf{1} \quad \text{lefthanded} \tag{2.20}$$

$$\sum_{j_m=1}^{d} A^{[M]j_M}_\rightarrow(A^{[M]j_M}_\rightarrow)^\dagger = \mathbf{1} \quad \text{righthanded} \tag{2.21}$$

If Eq. (2.20) applies to all matrices $A^{[m]j_m}$ with $1 < m \leq k$, then the left block states $|\Phi^{[A]}_{\alpha_k}\rangle$ orthonormality can be established,by its successive use (after using the

boundary 2.20). The same occurs for the right block states $|\Phi^{[B]}_{\alpha_k}\rangle$, after applying Eq. (2.21).Finally, we now require $|\Psi\rangle$ to be normalised, which is equivalent to $tr(D^2) = 1 = \sum_{\alpha_k} \lambda^2_{\alpha_k} = 1$, allowing the diagonal matrix D to be identified with the matrix of Schmidt coefficients $\sqrt{\Lambda^{[k]}}$.

2.4 Calculations with MPS

2.4.1 Density matrices

In order to produce any measure it's necessary define the reduced density operators of a small subset of sites, such as ρ_k for a single site k or ρ_{kl} for two sites k and l, and expectation values of the form $\langle\Psi|O_1 \otimes O_2 \cdots O_M|\Psi\rangle$ where $\{O_j\}_{j=1}^M$ are operators acting in the Hillbert space $\mathcal{H}_j$ of site j. For convenience the description given for the rest of this section utilises MPS with PBC and unconstrained matrices. To begin the full density operator $\rho = |\Psi\rangle\langle\Psi|$ of the system is given by

$$\rho \quad = \quad \sum_{J_{[1,M]}} \sum_{I_{[1,M]}} tr\Big(\prod_{m=1}^{M} A^{[m]j_m}\Big) tr\Big(\prod_{m=1}^{M} A^{*[m]j_m}\Big) |J_{[1,M]}\rangle\langle I_{[1,M]}| \tag{2.22}$$

after using $tr(XYZ)^* = tr(X^*Y^*Z^*)$.By applying the matrix identities$tr(X)tr(Y) = tr(X \otimes Y) = tr(Y \otimes X)$and $(ABC) \otimes (XYZ)$ =$(A \otimes X)(B \otimes Y)(C \otimes Z)$we obtain a more compact form

$$\rho \quad = \quad \sum_{J_{[1,M]}} \sum_{I_{[1,M]}} tr\Big(\prod_{m=1}^{M} E^{[m]j_m i_m}\Big) |J_{[1,M]}\rangle\langle I_{[1,M]}| \tag{2.23}$$

where $E^{[m]j_m i_m} = A^{[m]j_m} \otimes A^{*[m]i_m}$. To normalize the state we trace out all the physical sites as $tr(\rho) = \langle\Psi|\Psi\rangle = tr(\prod_{m=1}^{M} I^{[m]})$ where the contraction of the physical indices labelling the set of matrix $E^{[m]j_m i_m}$ is called the "transfer" matrix and is denoted as $I[m] = \prod_{j_m=1}^{d} E^{[m]j_m j_m}$. By leaving out one site k from this trace we obtain the reduced density operator

$$\rho_k \quad = \quad \sum_{j_k=1}^{d} \sum_{i_k=1}^{d} tr\Big(\Big[\prod_{m=1}^{k-1} I^{[m]}\Big] E^{[k]j_k i_k} \Big[\prod_{m'=k+1}^{M} I^{*[m']}\Big]\Big) |j_m\rangle\langle i_m| \tag{2.24}$$

which is reproduced in fig(2.1). Expressions for the reduced density operators of larger numbers of sites then follow a similar form as a trace of products of appropriate sets of $I^{[m]}$ and $E^{[m]j_m i_m}$ matrices

$$\langle\Psi|O_1 \otimes O_2 \otimes \cdots O_M|\Psi\rangle = \quad tr\Big(\prod_{m=1}^{M} O^{[m]}\Big) \tag{2.25}$$

with the observable matrices being defined as

$$O^{[m]} = \sum_{j_m=1}^{d}\sum_{i_m=1}^{d}\langle j_m|O^m|i_m\rangle E[m]^{j_m i_m} \tag{2.26}$$

and noting that whenever $O_m = [1]_m$ then $O^{[m]} = I^{[m]}$.

2.4.2 Two-sites gates

Now we can move forward the essential core method of the TEBD algorithm, precisely how to update them after applying two-site gates. To begin we need only consider an MPS with the initial form

$$\rho_k \quad = \quad \sum_{J_{[1,M]}}\langle\Phi_0|\Big(\prod_{m=1}^{k-1} A_{\leftarrow}^{[m]j_m j_{m'}}\Big)\Xi^{j_k j_{k+1}}\Big(\prod_{m'=k+2}^{M} A^{[m']}\Big)|\Phi_m\rangle|J_{[1,M]}\rangle \tag{2.27}$$

where the A matrices are orthonormalised. The central set of matrices $\Theta^{j_k j_{k+1}}$ spanning the two sites is defined in one of three ways

$$\Xi^{j_k j_{k+1}}\begin{cases}\sqrt{\Lambda^{k-1}}A_{\rightarrow}^{[k]j_k}A_{\rightarrow}^{[k+1]j_{k+1}} & \text{Left ,}\\ A_{\leftarrow}^{[k]j_k}\sqrt{\Lambda^{k}}A_{\rightarrow}^{[k+1]j_{k+1}} & \text{Center}\\ A_{\leftarrow}^{[k]j_k}A_{\leftarrow}^{[k+1]j_{k+1}}\sqrt{\Lambda^{k+1}} & \text{Right}\end{cases} \tag{2.28}$$

depending on where the twist in the handedness is located. Since the remaining matrix products give orthonormalised left and right Schmidt states the state can be expressed in the basis

$$|\Psi\rangle = \sum_{[k,k+1]}\sum_{\alpha_{k-1}=1}^{\chi_{k-1}}\sum_{\alpha_{k+k1}=1}^{\chi_{k+1}}\langle\alpha_{k-1}|\Xi^{j_k j_{k+1}}|\alpha_{k+1}\rangle|L_{\alpha_{k-1}}^{[k-1]}\rangle|j_l\rangle|j_{j_{k+1}}\rangle|R_{\alpha_{k+1}}^{[k+1]}\rangle \tag{2.29}$$

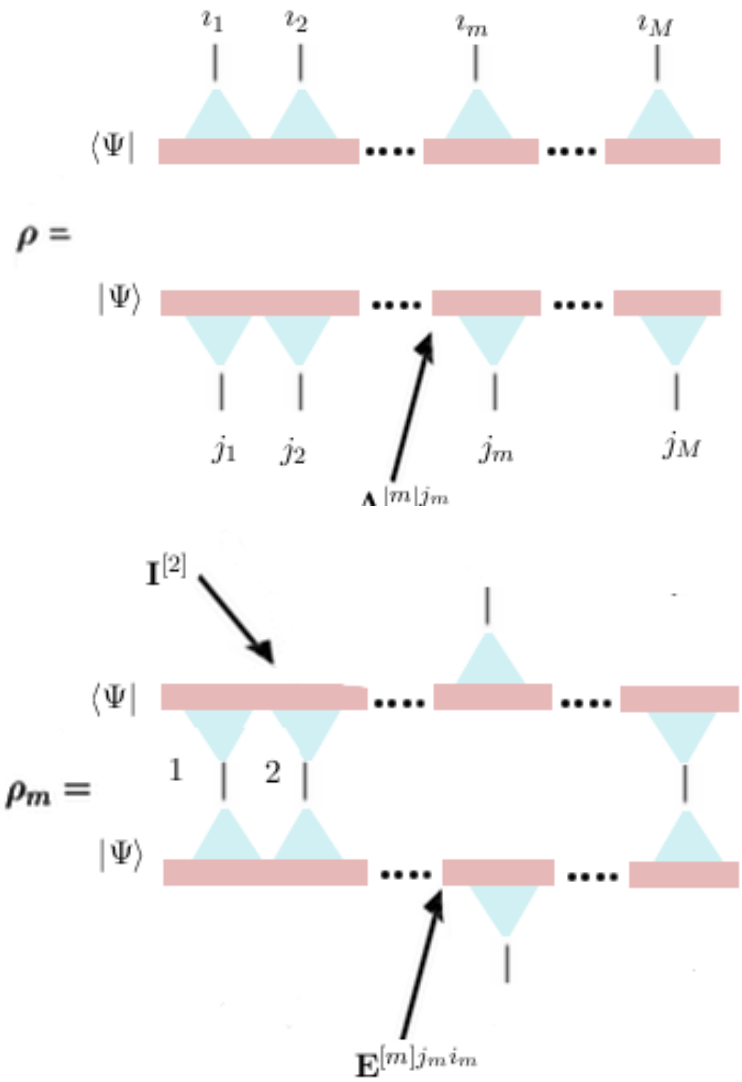

Figura 2.1: (a) The graphical representation of the full density matrix$\rho = |\Psi\rangle\langle\Psi|$ of the system with PBC. The shaded triangular object represents the matrices $A^{[m]j_m}$. (b) Tracing out all sites, aside from site m, is equivalent to contracting (joining) all the appropriate physical indices. The remaining (uncontracted) indices i_m and j_m are then the rows and columns of the density matrix ρ_m .The shaded objects represent the matrices $E^{[m]j_m i_m}$ and $I^{[m]}$.

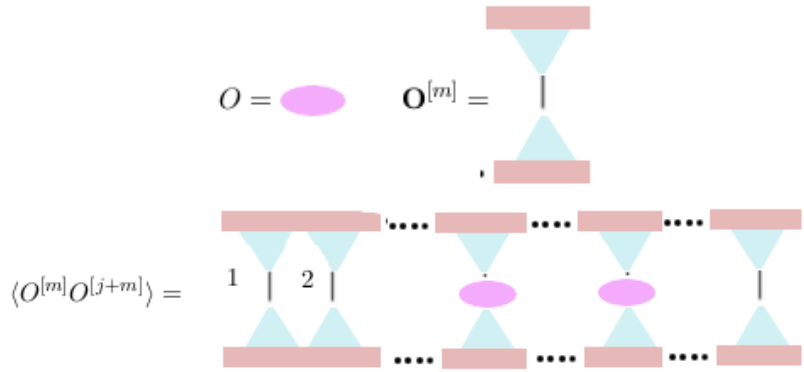

Figura 2.2: (a) An observable O acting on one site. (b) The graphical representation of the matrix $O^{[m]}$ formed by contraction with O. (c) The contraction of indices required for the computation of $\langle O^m O^{m+l} \rangle$.

The utility of this two-site-two-block form is that the physical basis of sites k and $k+1$ appear explicitly and we may now apply *exactly* an arbitrary transformation

$$\mathbf{G} = \sum_{J_{[k,k+1]}} \sum_{I_{[k,k+1]}} G^{j_k j_{k+1}}_{i_k i_{k+1}} |j_k\rangle |i_{k+1}\rangle \langle i_{k+1}| \langle j_{k+1}| \tag{2.30}$$

on these two sites directly. This transformation mixes up the set of $\Theta^{j_k j_{k+1}}$matrices as

$$\Theta^{j_j j_{k+a}} = \sum_{i_{k,k+1}} G^{j_k j_{k+1}}_{i_k i_{k+1}} \Xi^{i_k, i_{k+1}} \tag{2.31}$$

giving the new state $|\Psi'\rangle = \mathbf{G}|\Psi\rangle$ in the same basis as

$$|\Psi'\rangle = \sum_{[k,k+1]} \sum_{\alpha_{k-1}=1}^{\chi_{k-1}} \sum_{\alpha_{k+k1}=1}^{\chi_{k+1}} \langle \alpha_{k-1} | \Theta^{j_k j_{k+1}} | \alpha_{k+1} \rangle | L^{[k-1]}_{\alpha_{k-1}} \rangle | j_l \rangle | j_{j_{k+1}} \rangle | R^{[k+1]}_{\alpha_{k+1}} \rangle \tag{2.32}$$

which is shown in Fig. (a). In a similar way to $\Xi^{j_k j_{k+1}}$ the new quantity $\Theta^{j_k j_{k+1}}$ is a set of $d^2(\chi_{k-1} \times \chi_{k+1})$ matrices indexed by the two physical indices j_k and j_{k+1}. This matrix represents a set of anomalous two-site matrices in our MPS. To bring the decomposition back into a standard MPS form we need to factorise $\Theta^{j_k j_{k+1}}$. A technical description of this procedure can be found in the mathematical extra.

Capitolo 3

Time Evolving Block Decimation

As stated at the beginning the biological system are slightly entangled one so we only consider Hamiltonians with nearest neighbouring interactions,therefor we have an explicit 1D geometry. The most general form of Hamiltonian we shall consider is

For OBC it is convenient both for notation and for calculations to reformulate $H(t)$ in terms of time-dependent two-site operators as

$$H_{j,j+1} = \frac{1}{2}\sum_{\nu=1}^{k_1} c_j^{\nu}(t)h_j^{\nu} + \sum_{\nu=1}^{k_2} c_j^{\nu}(t)h_{j,j+1}^{\nu} + \frac{1}{2}\sum_{\nu=1}^{k_1} c_{j+1}^{\nu}(t)h_{j+1}\nu \qquad 1 \leq j \leq M-1 \quad (3.1)$$

which are defined symmetrically about site j, aside from at the boundaries where

$$H_{1,2}(t) = \sum_{\nu=1}^{k_1} c_j^{\nu}(t)h_j^{\nu} + \sum_{\nu=1}^{k_2} c_j^{\nu}(t)h_{j,j+1}^{\nu} + \frac{1}{2}\sum_{\nu=1}^{k_1} c_{j+1}^{\nu}(t)h_{j+1}\nu$$

$$H_{M-1,M}(t) = \sum_{\nu=1}^{k_1} c_j^{\nu}(t)h_j^{\nu} + \sum_{\nu=1}^{k_2} c_j^{\nu}(t)h_{j,j+1}^{\nu} + \frac{1}{2}\sum_{\nu=1}^{k_1} c_{j+1}^{\nu}(t)h_{j+1}\nu$$

giving in total $H(t) = \sum_{j=1}^{M-1} H_{j,j+1}(t)$. We search for the dynamical evolution of a system given by the integration of dimensionless time-dependent Schrodinger equation $\imath\delta_t|\Psi(t)\rangle = H(t)|\Psi\rangle$. For the case of a time-independent Hamiltonian H this equation admits a formal solution $|\Psi(t)\rangle = \exp^{(-iHt)}|\Psi\rangle$. Numerical calculations proceed by discretising the total time T into $T/\delta t$ steps where $\delta t \leq 1$ as $t_n = (n-1)\delta t$ with $n = (1, \cdots, T/\delta t)$, obtaining the time-evolution operator$U(t)$ as the product

$U(t) = \prod_{n=1}^{t} exp(-iH(t_n)\delta t)$ connecting the initial state$|\Psi\rangle$ to the state $|\Psi(t)\rangle$. The computation of U_n is further aided by the nearest neighbour hypothesis,the latter enables $H(t_n)$ to be summed up into two operators $H(t_n) = F + G$ where

$$F = \sum_{oddj} H_{j,j+1}(t_n) \quad \text{and} \quad G = \sum_{evenj+1} H_{j,j+1}(t_n) \tag{3.2}$$

leaving $U_n = exp[-i(F + G)\delta t]$. Since no two terms within either F or G involve the same sites they all commute amongst themselves. Given that the exponential of each operators alone can be calculated exactly as the product of unitaries which act exclusively on two neighbouring sites

$$e^{-iF\delta t} = \prod_{oddj} e^{-iH_{j,j+1(t_n)\delta t}} \quad \text{and} \quad e^{-iG\delta t} = \prod_{evenj} e^{-iH_{j,j+1(t_n)\delta t}} \tag{3.3}$$

The complications in computing the unitary U_n fully arise from the fact that F and G do not in general commute. Thanks the Suzuki-Trotter expansion we ensure the preservation of the norm of the state and we can overcome the problem of the commutation of the exponential of our evolution operators.

The simplest and more common expansion follows by assuming F and G commute and constitutes a first-order expansion of U_n in δt as $U_n = exp(-iF\delta t)exp(-iG\delta t)+ O(\delta t^2)$. If instead we define the symmetric product

$$s(F, G, y) = e^{-\frac{1}{2}iFy} e^{-iGy} e^{-\frac{1}{2}iFy} \tag{3.4}$$

then a second-order expansion follows as $U_n = s(F, G, \delta t) + O(\delta t^t 3)$. Important to set: Trotter error is not the only source of error and in most cases is actually the least important. For this reason using higher-order expansions can even become counter-productive.

3.0.3 Suzuki-Trotter sweeps

The suzuki Trotter decomposition is performed applying a two-site gate to an even and odd sites. In order to start the ST sweep and apply the gate operator we

have to ensure that the handedness of all matrices A of the initial state is the same, for example left-handed : $A_{\leftarrow}^{[1]j_1} A_{\leftarrow}^{[2]j_2} \cdots A_{\leftarrow}^{[M]j_M}$. Given that we can apply to the two sites (eq 2.28,2.29) the gate of the formula 2.30 in order to compute the $n-th$ time step evolution of $F_{j,j+1}$ or $G_{j+1,j+2}$. Problem lies in the fact that after applying the unitary gate the updated matrix $A^[k]$ posses the correct handedness ($\leftarrow$)while the $A^[k+1]$ doesn't($\rightarrow$), but it can be flipped to $A_{\leftarrow}^{'[k+1]}$ via a right division by $\sqrt{\Lambda^{[k+1]}}$ and a left multiplication by $\sqrt{\Lambda^{[k]}}$. Despite it's facility, this operation it's numerical unstable being the value of $\sqrt{\Lambda^{[k+1]}}$ very small. This means that a tentative of higher our precision in the simulation raising the value of χ, if excessive, will enhance the numerical instability. In every case this problem can be solved by applying the gates in sequential zip.For example, in the case of a second-order decomposition acting on a state which is entirely lefthanded we apply the gates within $exp(-iF\delta t)$ from left-to-right as

$$\begin{aligned} e^{-\frac{1}{2}iF\delta t} &= e^{-\frac{1}{2}iH_{1,2}(t_n)\delta t}(\mathbf{1}_{2,3})e^{-\frac{1}{2}iH_{3,4}(t_n)\delta t} \cdot \\ &\quad \cdot(\mathbf{1}_{4,5}) \cdots (\mathbf{1}_{M-2,M-1})e^{-\frac{1}{2}iH_{M-1,M}(t_n)\delta t} \end{aligned} \tag{3.5}$$

where explicit identity operations $_{k,k+1}$ have been inserted in between the usual unitaries. The purpose of the identity operations is to shift the twist in handedness one site to the right making the decomposition compatible for the next gate. We then do precisely the same, but in the opposite direction, when applying $exp(-iG\delta t)$, and finally after applying the last zip $exp(-iF\delta t)$ our MPS will be entirely righthanded. We remark here that this kind of zipping is very close to the finite-system sweeps used in DMRG.

3.1 Errors in TEBD

3.1.1 Trotter Error

For any single time-step δt the Trotter error $\epsilon_{\delta t}$ will be of order $\epsilon_{\delta t} \approx (\delta t)^{p+1}$ for a pth- order expansion. To evolve the state to some final time T we need to perform $T/\delta t$ time steps, and denote the state after these steps as $|\Psi_{st}\rangle$. If the exact time-

evolved state is $|\Psi(T)\rangle$ then the Suzuki-Trotter overlap error is $\epsilon_{st} = 1 - |\langle\Psi(T)|\Psi_{st}\rangle\ |$. It has been found from numerical evidence [9] that $\epsilon_{st} \approx MT(\delta t)^p$ and therefore scales linearly with the overall evolution time T and the system size M. This error is controlled entirely by δt and so requires $\delta t << 1$.

3.1.2 Truncation error

The most important source of error in TEBD is the truncation of this Schmidt decomposition to include only the χ Schmidt states with the largest Schmidt coefficients. This source of errors derive from the truncation approximation of the state $|\Psi\rangle = |\Psi_{tr}\rangle - |\Psi_{res}\rangle$, with $|\Psi_{tr}\rangle = \sum_{\alpha_m}^{\chi} \lambda_{\alpha_m}^{[m]} |L_{\alpha_m}^{[m]}\rangle |R_{\alpha_m}^{[m]}\rangle$ and $|\Psi^{\perp}\rangle = \sum_{\alpha_m > \chi} \lambda_{\alpha_m}^{[m]} |L_{\alpha_m}^{[m]}\rangle |R_{\alpha_m}^{[m]}\rangle$.

At the first step we have $\epsilon_m = 1 - |\langle\Psi|\Psi_{res}\rangle| = \sum_{\alpha_m > \chi} (\lambda_{\alpha_m}^{[m]})^2$. At the next step we will decompose the state $|\Psi_{res}\rangle$ in the same way obtaining a total error $\epsilon_{m+1} = 1 - |\langle\Psi|\Psi_{res}^{'}\rangle = 1 - (1 - \epsilon_{m+1} - \epsilon_m)$. So moving along all the sites the final truncation error will be $\epsilon_{tr} = \sum_{m=1}^{M-1} \epsilon_m$ which is additive in the individual truncation errors. In practise the degradation of the norm of the MPS is a good measure of the truncation error and we might tolerate it becoming 10^{-6}.

The runaway time was empirically found to increase with χ, but decreases with the number of two- site gates applied and with M. Obtaining an accurate simulation for a desired time therefore requires a careful balancing of δt and the order of the Suzuki-Trotter expansion.

Here a graph of the effects of the runaway time effects for an application of 1000 two-site gate application

Here we can see the direct effect of the refinement of the value of our basis trough the rising of the χ parameter inside our simulation. As stated above a low value of the Schmidt basis will give raise to numerical instability for a very low run away time. A χ value of 30 just show to better preserve the norm (and so the dynamics) from great instability.

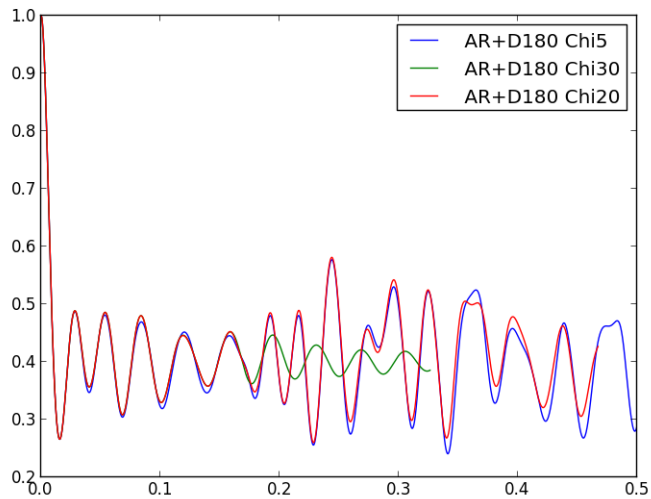

chi5-20-30.png

Figura 3.1: Populations for AR spectra + delta $180cm^{-1}$; rising up of population caused by truncation error at a valuable runaway time for small χ and different effects on the dynamics by the truncation error

Capitolo 4

Mapping between system-reservoir quantum models and semi-infinite discrete chains

4.1 Introduction

All quantum systems encountered in nature experience random perturbations due to their coupling to degrees of freedom of their local environments. Information about these degrees of freedom are not normally accessible, and to correctly predict the results of experiments, these degrees of freedom must be averaged over. This averaging introduces qualitatively new features into the otherwise unitary dynamics of the quantum system, and typically induces an effectively irreversible dynamics which drives the system towards an equilibrium with its environment.For quantum systems, this evolution towards equilibrium not only involves energy transfer to the environment, but can also cause the loss of coherence in the system state, often on a much faster timescale than the energy relaxation. This latter process of decoherence destroys quantum mechanical effects arising from the existence of phase coherence in the state of the system, and must be a part of the total correct dynamics of every phenomena description.. The most simple model is the Spin-Boson Model (SBM) one of the simplest non-trivial models of open-system dynamics. This model describes a single two-level system (TLS) coupled linearly to the coordinates of an environment consisting of a continuum of harmonic oscillators and despite its simplicity, this model shows a rich array of non-Markovian dynamical phenomena

that for so short time events can became of relevant importance. In the case of Quantum Biology this non Markovian backward effects of interaction due to the system environment coupling are the key element of the lasting of coherence into the system (see next chapter).The action of the orthogonal polynomials is to project by unitary transformation the Hamiltonian into the normal vibrational modes coordinates and produce the 1D chain useful for our dynamical simulation without any need of discretisation.

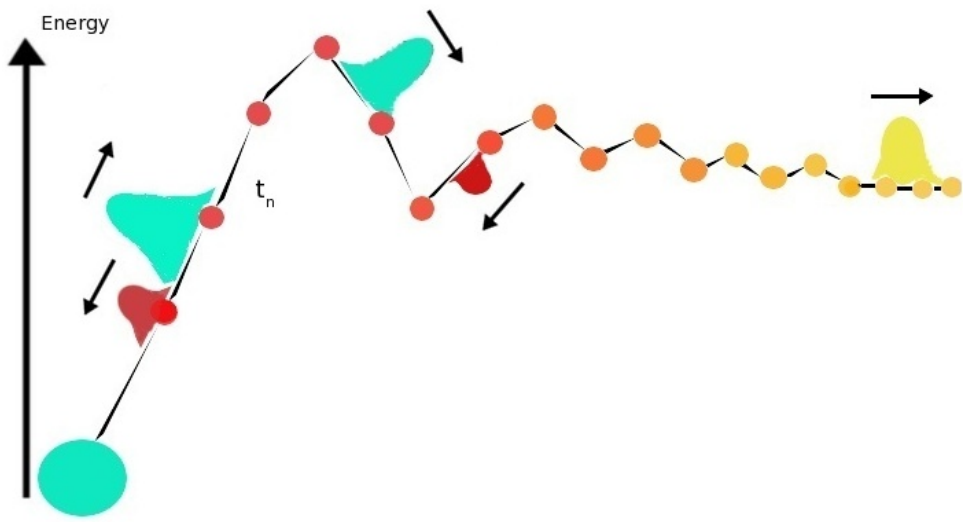

Figura 4.1: pictorial representation of the back scattering effect behind the reborn of coherence into the system for an inhomogenous chain

As depicted in fig (3.1) the type of chain product from the projection operator isn't translationally invariant, in this way optical effect of reflection can take place and produce back scattering energy that will come back into the system. Subsystem initially injects excitations (shown as wave packets) into inhomogenous region of the chain. Scattering from inhomogeneity causes back action of excitations on the system at later times and leads to memory effects and non-Markovian subsystem dynamics. At long times (yellow dots), after multiple scattering the energy landscape smooths , excitations penetrate into the homogenous region and propagate away from the system without backscattering. This leads to irreversible and Markovian

excitation absorption by the environment. The inhomogeneity of the chain enter into the local hamiltonian modifying the energy local parameters of the system through a sort of

4.1.1 System Reservoir structure

The observables in an open quantum system are affected by the unavoidable interaction with the environment. This environment may be described by an infinite number (often called a reservoir) of bosonic or femionic modes labeled by some real number. The internal dynamics of the reservoir is given by some Hamiltonian of the form

$$H_{res} = \int_0^{x_{max}} dx g(x) a_x^\dagger a_x \tag{4.1}$$

where in a physical context x could represent some continuous real variable such as the momentum of each mode, and x_{max} the maximum value of it which is present in the reservoir (it could be infinity). In this picture $g(x)$ represents the dispersion relation of the reservoir which relates the oscillator frequency to the variable x. The creation and annihilation operators satisfy the continuum bosonic $[a_x, a_y^\dagger] = \delta(x-y)$ or fermionic $\{a_x, a_y^\dagger\} = \delta(x?y)$ commutation rules. We assume that the frequencies $g(x)$ and momenta x of the reservoir are bounded. The internal dynamics of the open quantum system are described by a un- specified local Hamiltonian operator H_loc and we assume that the interaction between the system and the reservoir is given by a linear coupling

$$v = \int_0^{x_{max}} dh h(x) \hat{A}(a_x^\dagger a_x) \tag{4.2}$$

where $\hat{A}$ is The internal dynamics of the open quantum system are described by a un- specified local Hamiltonian operator Hloc and we assume that the interaction between the system and the reservoir is given by a linear coupling.

$$H = H_{loc} + H_{res} + V = H_{loc} + \int_0^{x_{max}} dx g(x) a_x^\dagger a_x + \int_0^{x_{max}} dx h(x) \hat{A}(a_x^\dagger + a_x) \tag{4.3}$$

It has been shown that the dynamics induced in the quantum system by its interaction with the reservoir is completely determined by a positive function of the

energy (or frequency ω) of the oscillators called the spectral density $J(\omega)$. For the continuum model of the reservoir we are considering, this function is given by

$$J(\omega) = \pi h^2[g^{-1}(\omega)]\frac{dg^{-1}((\omega)}{d\omega} \tag{4.4}$$

where $g^{-1}[g(x)] = g[g^{-1}(x)] = x$. Physically $\frac{dg^{-1}((\omega)}{d\omega}$ can be interpreted as $d\omega$ the number of quanta with frequencies between ω and $\omega + \delta\omega$ as $\delta\omega \to 0$ it represents the density of states of the reservoir in frequency space. The spectral function thus describes the overall strength of the interaction of the system with the reservoir modes of frequency ω. This physical introduction motivate the next mathematical definition.

Definition. It's defined as spectral density of a reservoir as a real non- negative and integrable function $J(\omega)$ inside of its (real positive) domain, which could be the entire half-line $\omega \in [0, \infty)$. Of course, given only a spectral density $J(\omega)$), the dispersion relation $g(x)$ and the coupling function $h(x)$ are not uniquely defined. We shall make use of this freedom to implement a particularly simple transformation of the bosonic modes, and we will chose the dispersion function to be linear $g(x) = gx$. Our main theorem is

Theorem 3.1 *A system linearly coupled with a reservoir characterized by a spectral density $J(\omega)$ is unitarily equivalent to semi-infinite chain with only nearest-neighbors interactions, where the system only couples to the first site in the chain. In other words, there exist an unitary operator $U_n(x)$ such that the countably infinite set of new operators*

$$b_n^\dagger = \int_0^{x_{max}} dx U_n(x) a_x^\dagger$$

satisfy the corresponding commutation relations $[b_n, b_m^\dagger] = \delta_{nm}$ for bosons, and $\{b_n, b_m^\dagger\} = \delta_{nm}$ for fermions, with transformed Hamiltonian

$$H' = \int_0^{x_{max}} dx U_n(x) H = H_l oc + c_0 \hat{A}(b_0 + b_0^\dagger) + \sum_{n=0}^{\infty} \omega_n b_n^\dagger b_n + t_n b_{n+1}^\dagger b_n + t b_n^\dagger b_{n+1} \tag{4.5}$$

where c_0, t_n, ω_n are real constants.

Proof. The proof is by construction. Since $J(\omega)$ is positive, $h(x)$ is real, this defines

the measure $d\mu(x) = h^2(x)dx$. Then write

$$U_n(x) = h(x)\tilde{p}(x) = h(x)\frac{\pi_n}{||\pi_n||}(x) \tag{4.6}$$

where $\tilde{p}_n(x)$ are some set of orthonormal polynomials with respect to the measure $d\mu(x) = h^2(x)dx$ with support on $[0, x_{max}]$. Then it is clear that Un(x) is unitary (actually orthogonal as it is also a real transformation) in the sense of

$$\int_0^{x_{max}} dxU_n(x)U_m^\star(x) = \int_0^{x_{max}} dxU_n(x = U_m(x) = \int_0^{x_{max}} \tilde{p}_n(x)\tilde{p}_m(x) = \delta_{nm} \tag{4.7}$$

so the inverse transformation is just

$$a_x^\dagger = \sum_n U_n(x)b_n^\dagger \tag{4.8}$$

Moreover for bosons

$$\begin{aligned}
[b_n, b_m^\dagger] &= \int_0^{x_{max}}\int_0^{x_{max}} dxdx'U_n(x)U_m(x')[a_x, a_{x'}\dagger] \\
&= \int_0^{x_{max}}\int_0^{x_{max}} dxdx'U_n(x)U_m(x')\delta(x-x') \\
&= \int_0^{x_{max}} dxU_n(x)U_m(x) = \delta_{nm}
\end{aligned}$$

and similarly it is proved that $\{b_n, b^dagger_m\} = \delta_{nm}$ for fermions. It remains to determine the structure of the transformed Hamiltonian H, note that V is transformed like:

$$V = \hat{A}\sum_n \int_0^{x_{max}} dxh(x)U_n(x)(b_n + b_n^\dagger) = \quad \hat{A}\sum_n \int_0^{x_{max}} dxh^2(x)\frac{\pi_n(x)}{||\pi_n||}(b_n + b_n^\dagger)$$

since for monic polynomials $\pi_0(x) = 1$ we find

$$\begin{aligned}
V &= \hat{A}\sum_n \int_0^{x_{max}} dxh^2(x)\frac{\pi_n(x)}{||\pi_n||}(b_n + b_n^\dagger) \\
&= \hat{A}\sum_n \frac{||\pi_n||^2\sigma_{n0}}{||\pi_n||}(b_n + b_n^\dagger) = ||\pi_0||\hat{A}(b_0 + b_0^\dagger)
\end{aligned}$$

so $c_0 = ||\pi_0||$. For the H_res term, note that with the choice of lineaer dispersion function $g(x) = gx$ for the spectral density $J(\omega)$ one obtains

$$\begin{aligned} H_{res} = \sum_{n,m} \int_0^{x_{max}} dx g(x) U_n(x) U_m(x) b_n^\dagger b_m \\ &= \sum_{n,m} \int_0^{x_{max}} dx h^2(x) g(x) \tilde{p}_n(x) \tilde{p}_m(x) b_n^\dagger b_m \\ &= g \sum_{n,m} \int_0^{x_{max}} dx x h^2(x) \tilde{p}_n(x) \tilde{p}_m(x) b_n^\dagger b_m \end{aligned}$$

With the recurrence relation we substitute the value of $x\tilde{p}_n(x)$ in the above integral to find

$$H'_{res} = g \sum_{n,m} \int_0^{x_{max}} dx h^2(x) \Big[\frac{1}{C_n} \tilde{p}_{n+1}(x) + \frac{A_n}{C_n} \tilde{p}_n(x) + \frac{B_n}{C_n} \tilde{p}_{n-1}(x) \Big] \tilde{p}_m(x) b_n^\dagger b_m \quad (4.9)$$

then orthonormality yields

$$\begin{aligned} H'_{res} &= g \sum_n \frac{1}{C_n} b_n^\dagger b_{n+1} + \frac{A_n}{C_n} b_b^\dagger b_n + \frac{b_{n+1}}{C_{n+1}} b_{n+1}^\dagger b_n \\ &= g \sum_n \sqrt{\beta_{n+1}} b_n^\dagger b_{n+1} + \alpha b_n^\dagger b_n + \sqrt{\beta_{n+1}} b_{n+1}^\dagger b_n \end{aligned}$$

where we have used the relation between monic and orthogonal recurrence coefficients. So finally we have

$$\omega_n = g\alpha_n$$
$$t_n = g\sqrt{\beta_{n+1}}$$

4.1.2 Applications

As a prototypical example let us consider the spin-boson Hamiltonian which describes the interaction of a TLS with an environment of harmonic oscillators

$$H_{SB} = H_{loc} + \int_0^{x_{MAX}} dx g(x) a_x^\dagger a_x + \frac{1}{2}\sigma_3 \int_0^{x_{MAX}} dx h(x) (a_x^\dagger a_x) \quad (4.10)$$

where a_x are bosonic operators, and the local Hamiltonina of the spin is ginve by

$$h_{loc} = \frac{1}{2}\eta\sigma_1 + \frac{1}{2}\epsilon\sigma_3 \quad (4.11)$$

where σ_1, σ_2 are the corresponding Pauli matrices. Firstly we will consider spectral functions bounded by a hard cut-off at an energy ω_c, hence the cut-off $x_{max} = g?1(\omega_c)$ appearing in the integrals in, which are usually parameterized as

$$J(\omega) = 2\pi\alpha\omega_c^{1-s}\omega^s(\omega - \omega_c) \tag{4.12}$$

where α is the dimensionless coupling strength of the system-bath interaction and $\theta(\omega - \omega_c)$ denotes the Heaviside step function. In the SBM literature, spectral functions with $s > 1$ are referred to as super-ohmic, $s = 1$ as Ohmic, and $s < 1$ as sub-Ohmic. According to and our convention in taking linear dispersion relations, this continuous spectral function is related to the Hamiltonian parameters by

$$g(x) = \omega_c x \qquad h(x) = \sqrt{2\alpha}\omega_c x^{s/2} \tag{4.13}$$

With this choice of $g(x)$ and $h(x)$, $x_{max} = 1$ and absorbing the common factor $\omega_c\sqrt{2\alpha}$ in the system operator $A = \omega_c\sqrt{2\alpha}\sigma_3$, the following matrix elements generate the mapping onto the chain

$$U_n = x^{s/2}\bar{P}_n^{(0,s)}(x) \tag{4.14}$$

here $\bar{P}_n^{(0,s)} = P_n^{(0,s)(x)N_n^{-1}}$ is a (normalized) shifted Jacobi polynomial (from support [-1,1] to support [0,1]) . The straight calculation can can be found in the mathematical extras What we care in our simulation is the final result

$$\omega_n = \omega_c(2n + 1 + s) \tag{4.15}$$

$$t_n = \omega_c\sqrt{(n + 1)(n + s + 1)} \tag{4.16}$$

that once introduced into our simulation performed the variation in local site energies and hopping along the chain of normal modes. In this way we reproduce the local site variation energy of the (quantum) system and the tunneling parameters along the chain to reproduce the dynamics of the OQS. Obviously in a simulation the setting of parameters can affect enormously the final result, and in order to correctly describe the dynamic simulation of a system we must be aware of these effects. The two most

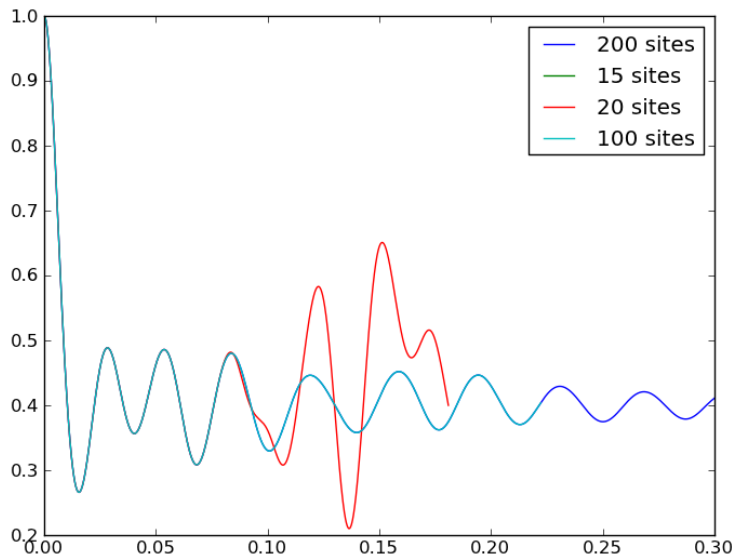

Figura 4.2: backward propagation effects on the population dynamcs on sites 1 of the clorophilla antenna of theBb820 RC, in the initial state as exciton state, due to different chain lenght. Initial valueχ= 30, number of bosons=9

significant one are the variation of the total number of boson parameter applied in our simulation and the total length of the chain we used in our modellisation.

In figure 3.1 we can see the great difference in the dynamics behaviours between too much short chains (15 and 20 sites) which produce unavoidable border effect (that resemble a lot the numerical instability of figure 2.3 for short appearances of the runaway time) and longer chains (we can see great difference just starting with a chain of length 100).

while here in fig 3.3 we can see how little variation doesn't produce any particular difference for certain time evolution. Usually the greater the number of projection the better, if not the only problem connected are numerical one, in the maintenance of numerical stability in the ORTHOPOL connected with the use of Stieltjes integral in order to produce our desiderata new energies and tunnelings values. So we always must make the correct compromise between parameters' value inside the numerical

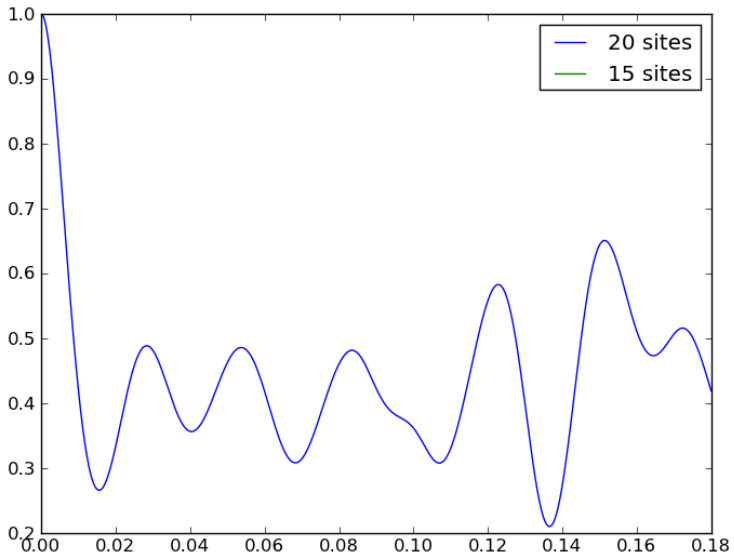

Figura 4.3: backward propagation effects on the population on sites 1 of the clorophilla antenna of theBb820 RC for comparable length chain.initial valueχ= 30, number of bosons=9

possibilities ours tools permit us. A shorter chain will not be affected from numerical instability connected to the Stieltjes integrations but will suffer of great border effects, while in the other case the dynamics will not suffer borders effects but should be wrecked from previous instabilities.

Here we can check the numerical difference between physical systems treated with a different number of bosons, but with same χ and length of 200

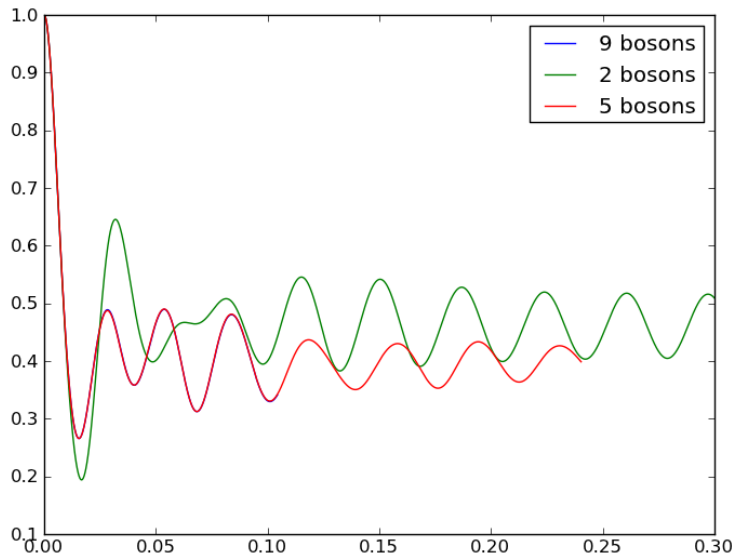

Figura 4.4: dynamics with different boson number for the modellisation of the phonon environment.χ=30 chain lenght of 200

Capitolo 5

Photosynthesis network transport

5.1 The phonon antenna mechanism

The extreme consequence of the basic principle of phonon antenna have been found to underlie the fruitful interplay between vibrational environments and coherent quantum dynamics, which will provide an understanding why optimal transport performance in proteic complex can arise at intermediate noise levels. As example let's use a 3 sites network where site 2 whose excitation energy, position and orientation, and hence dipolar interaction strength with sites 1 and 3 we are free to choose. We assume that site 3 provides the zero of excitation energy, the question that we would like to answer concerns the optimal choice of excitation energy, position and orientation of site 2 or in other words the optimal choice of the excitation energy of site 2 and its dipolar coupling strengths to sites 1 and 3 As such, this question cannot be answered unambiguously as we are missing a crucial piece of information, namely that of the structure of the environmental fluctuations. This structure is characterized by the spectral density of the environment which is a combination of the density of environmental modes and their individual coupling strength to the system. Let's assume that the environmental spectral density has a single maximum , roughly as depicted in fig.(4.1). We finds that the optimal position of site 2 is close to site 1 such that it exhibits a strong coherent dipolar interaction and close in excitation

energy. these have been found by numerical results, now we can rationalize its origin and thereby arrive at a very useful design principle of phonon antenna. Indeed, the

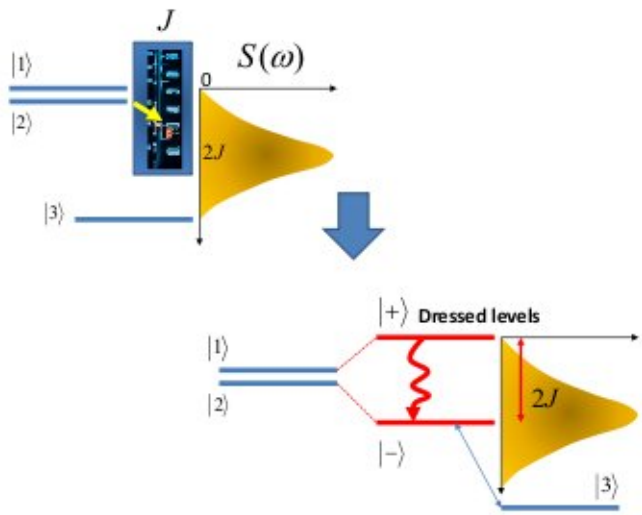

Figura 5.1: In the upper figure, two closely spaced energy levels are separated from a third level to which excitations should be delivered. They are subject to dephasing noise from an environment with a finite bandwidth that exhibits a maximum. A coherent interaction between the upper two energy levels leads to dressed states $|\pm\rangle$ with an energy splitting which, if matched to the maximum of the environment spectral density, will optimize transport from the upper to the lower level. Hence the dressed states act as an antenna to harvest environmental fluctuations to enhance transport.

strong coherent dipolar interaction between sites 1 and 2 suggests that we move to a new basis made up of the eigenstates of the coherent part of the dynamics of these two sites, that is the excitonic states of that system (for quantum opticians, the dressed state). This change of picture leads us to rewrite the Hamiltonian that describes the system-environment interaction$H_I = \frac{1}{2}\sum_n \left(\sum_h \sqrt{S_{nh}\omega_k(a_{nh} + a_{nh}^\dagger}|n\rangle\langle n|\right.$ in the excitonic basis of eigenstates $|e_n\rangle$ of eq. (1), so that $|i\rangle = \sum_n C_n^i |e_n\rangle$ and the coupling terms

$$H_I = \frac{1}{2}\sum_{n,m}(Q_{n,m}|e_n\rangle\langle e_m| + h.c.) \tag{5.1}$$

where

$$Q_{n,m} = \sum_{i,k}\sqrt{S_k}w_k C_n^i C_m^i (a_{ik} + a_{ik}^\dagger) \tag{5.2}$$

This leads us to two insights. Firstly, in the exciton basis the action of the dephasing noise now leads to transitions between excitons, that is amplitude noise, which

facilitates transport towards the lower of the two exciton states. Secondly, the two excitons (dressed states) are separated by an energy difference that is related to the coherent dipolar coupling strength and the energy difference of sites 1 and 2. The dominant contribution to the transition between these excitons (dressed states) arises from those environmental modes whose frequency closely matches the energy difference between dressed states. Indeed, it was found that the physically important relaxation pathway between sites 1 and 3 is mediated by pigments which are spectrally and spatially positioned by the protein to efficiently sample the spectral function of the proteins fluctuations

5.1.1 Non equilibrium long lived coherences

Experimental observations employing ultrafast 2-D spectroscopy on various photosynthetic complexes exhibited long-lived oscillatory features which were interpreted as evidence for long-lived electronic coherence in the systems under investigation [11][10]. Under this hypothesis electronic coherence appear to exhibit lifetimes that can reach the picosecond range thus exceeding expectations from condensed matter systems at least tenfold

5.1.2 Last overview on EET principles

The discovery of long-lived coherence between the singly excited electronic states of photosynthetic antenna complexes has necessitated both a rethinking of energy transfer in biological systems and, more broadly, a reconsideration of the role of the surrounding environment and of coherent dynamics in the condensed phase. These "persistent coherences" unexpectedly outlive coherences between the constituent singly excited states and the electronic ground state. An ever-growing body of work demonstrates the persistence of electronic coherence during energy transfer in a multitude of antenna complexes across broad phylogenic boundaries , and coherence within the Fenna-Matthews-Olson complex (FMO) has been shown to be robust to vibronic and structural modifications . This remarkable generality suggests that persistent electronic coherences may be a general property of any system of dense-

ly packed chromophores arranged in a nearly static relative geometry and coupled to a common bath. Despite numerous observations of persistent electronic coherence in photosynthetic systems, no clear microscopic mechanism for the survival of these coherences has been experimentally verified. Theoretical efforts to dissect the atomistic mechanism are complicated by the size and complexity of photosynthetic light-harvesting systems. Consequently, many competing models have been introduced to explain the observed quantum beating. These models invoke a broad range of physical mechanisms, including vibrational coherences , vibronic excitons, nonadiabatic couplings , correlated protein motion , nonsecular coupling between coherence and population , and long-range dielectric fluctuations [10]

The higher lying electronic levels, representing the various exciton eigenstates of the electronic system, are not excited even at room temperature as the excitation energy is in the range of eV. The initial (fast) injection of an exciton, either coherently or incoherently, populates one of the exciton states of the system and creates a sudden force on the electrons and nuclei and thus change their equilibrium positions . Now the environment will start to react to these forces which initiates transient oscillations of the modes at approximately their natural frequency w_k. The continuous background of the spectral density will relax very rapidly into the new equilibrium state as it contains a broad range of frequencies and thus possesses a very short correlation time. The well-defined long-lived vibrational mode will oscillate for a considerable time (which can be up to several picoseconds) and will interact with the electronic system. This in turn leads to oscillations between different exciton states. We make an observation: these oscillations will have the largest amplitude between those exciton states whose energy difference is nearly resonant with the frequency of the vibrational mode.

5.2 TEBD simulation for Dimeric system

5.2.1 Introduction

We have to keep in mind that one of the key messages of the preceding sections is the special role of the interplay between the quantum dynamics of a system and its environment, in particular when this environment does not merely represent white noise but possesses structure, and this is a typical characteristic of the biological type of environment. Furthermore, it has become clear that the optimal operating regime for quantum bio dynamics tends to favour parameter ranges in which the interaction between system components is comparable to the interaction of these system components and their environment. Both features are not well modeled by the traditional perturbative treatments that lead to master equations of Lindblad , Redfield or modified Red-field type . Indeed the essential importance of the non-Markovian nature of the system-environment interaction calls for the development of non-perturbative methods that can accurately, certifiably and efficiently model the resulting dynamics. From a numerical point of view it's important to remember that also for a standard model of open quantum system, as the just well commented spin-boson system, the dynamic induced in the quantum system it's strictly correlated to the structure of the distribution to which is coupled, which modellise all the information about the interaction between the quantum system and the environment. For the continuum model of the reservoire that we are considering i.e. choosing $g(x) = x$ this function is given by

$$J(\omega) = \pi h^2(\omega) \tag{5.3}$$

In other words the spectral function thus describes the overall strength of the interaction of the system with the reservoir modes of frequency ω. Despite it's relative simplicity, the dynamic of this model it's not exactly solveable and so we have to resort to numerical methods. This is even more true when the environmental spectral function exhibits considerable structure or when the coupling strength between system and environment lies in a non perturbative regime. This is exactly the set of

hypothesis we are moving on with our modelization, and even more. WE must remembering the reach and well structured environment of a biological system coupled to a quantum system that lies inevitably in a non perturbative regime, however even if the weight$h^2(x)$ is a complicated function, families of orthogonal polynomials can be found by using very stable numerical algorithms such as the ORTHOPOL package; in this way we are able to obtain a 1D system.This is the key that permit the deployment of the time-adaptive density matrix renormalization group (t-DMRG) technique to integrate the time evolution of the full system-environment dynamics efficiently.So now thank the interplay of this two methods we are able to couple our system (in this case our dimeric system) to environment which show different properties onto each site or adding also the local static-Gaussian- disorder in the site energies of the dimer,another quantity of of a certain relevance being used in the calculation for the optical spectra absorption of these proteic systems citeAR.

All this element, thanks to possibility to obtain a numerical precise simulation of the dynamics, concur to the simulation of a more and more realistic biological environment able to take advantage of it's quantum local properties.

5.2.2 Model parameters

All the data and simulations have been performed onto the modelisation of a proteic dimer (synthetic one or not). The quantum initial state used as initial state of the antenna sistem in the dimer was $\frac{1}{\sqrt{2}}\Big(|e\rangle_1 + |e\rangle_2\Big)$ (exciton state). The study on our dimeric system has been carried on zero temperature effect, so it means no thermal state is present, only the effect of the environmental spectral function have been taken into account into the simulations.The time scale is expressed 1/ 5.3 picosecond.

5.2.3 The Adolf-Rengel optical spectral

As stated above all the information of the interaction between the reservoire phonon bath and the local quantum system lies into the spectral density function

$J(\omega)$ of the exciton-vibrational coupling defined as

$$J(\omega) = \sum_{\epsilon} g_{\epsilon}\delta(\omega - \omega_{\epsilon}) \tag{5.4}$$

which is also a key quantity in the expressions for optical spectra and the rate constants for exciton relaxation discussed below. IN the standard theory and calculation the value $J(\omega)$ is assumed independent on the site index m; i.e., the same local modulation of site energies by the vibrational dynamics is assumed. As we will see through TEBD simulation it's possible to introduce the effect of different environment for each site, giving raise so to a broader variety of dynamics.

We will not undergo all the calculations developed to find the analytical form of the optical spectra, but we will check ourselves to the peculiar aspect of it.

The optical linear absorption is obtained from the dipole-dipole correlation function as explained in detail in Renger and Marcus

$$\alpha(\omega) \propto \Big\langle \sum_{M} |\mu_M|^2 D_M(\omega) \Big\rangle_{dis} \tag{5.5}$$

where $D_M(\omega)$ is the lineshape function and $\langle \quad \rangle_{dis}$ the denotes an average over static disorder in site energies. A Gaussian distribution function of width (FWHM) Δ_{dis} is assumed for these energies. The lineshape function $D_M(\omega)$ was obtained using a non-Markovian density matrix approach [13] . It is given as

$$D_M(\omega) = Re \int_0^{\infty} dt e^{\imath(\omega-\hat{\omega})t} e^{G_M(t)-G_M(0)} e^{t/\tau} \tag{5.6}$$

The value $D_M(\omega)$ contains both vibrational sidebands $G_M(t)$ and the lifetime broadening by the dephasing time τ_M.Both these quantities are related to $J(\omega)$. OF importance is the quantity $G_M(t)$ which is defined as

$$G(t) = \int_0^{\infty} dw[(1 + n(\omega)J(\omega)e^{-\imath\omega t} + n(\omega)J(\omega)e^{\imath\omega t}] \tag{5.7}$$

Where $n(\omega)$ is the mean number of vibrational quanta with energy $\hbar\omega$ that are excited at given temperature T.

The $\hat{\omega}$ source is shifted from the purely electronic transition frequency ω_M due to the exciton-vibrational coupling

$$\hat{\omega} = \omega_M - \gamma_{MM}\frac{E_\lambda}{\hbar} + \sum_{N\neq M} \gamma_{MN} C^{Im}(\omega_{MN}) \tag{5.8}$$

Here above appears another important quantities, the local reorganization energy E_λ defined as

$$E_\lambda = \hbar \int_0^\infty d\omega \omega J(\omega) \tag{5.9}$$

In the present model, the spectral density $J(\omega)$ contains both a broad low frequency contribution $S_0 J_0(\omega)$ by the protein vibrations with Huang-Rhys factor S_0 and a single effective high-energy vibrational mode of the pigments with Huang-Rhys factor S_H:

$$J(\omega) = S_0 J_0(\omega) + S_H \delta(\omega - \omega_H) \tag{5.10}$$

For the normalized low-frequency function $J_0(\omega)$ we assume that it has the same form as the spectral density, extracted recently [13] from 1.6 °K fluorescence line narrowing spectra of B777-complexes. The final lineshape function $D_M(\omega)$ so become

$$D_M(\omega) = e^{-S_H \gamma_{MM}} Re \int_0^\infty dt \sum_{k=0}^{\infty} \frac{(\gamma_{MM} S_H)^k}{k!} x e^{\imath(\omega - \hat{\omega_M} +)t} e^{G_M^0(t) - G_M^0(0)} e^{-t/\tau_M} \tag{5.11}$$

We obtained the typical figure.With Orthopol has been reproduced the shape of the AR figure summing the two part of the (5.2)

With TEBD it's also possible to handle the term ω of the purely electronic transition frequencies(or energies), of the final function $D_M(\omega)$, introducing a supplementary source of Gaussian static disorder into the local site energies.

Taking in account all the previous statements about structure environment and phonon antenna tuned on resonant peaks , we can add sharp delta function onto this standard function in order to take in account for all the resonant, local, typical phenomena. This is a first ,basic,example of different environments that act on different sites.

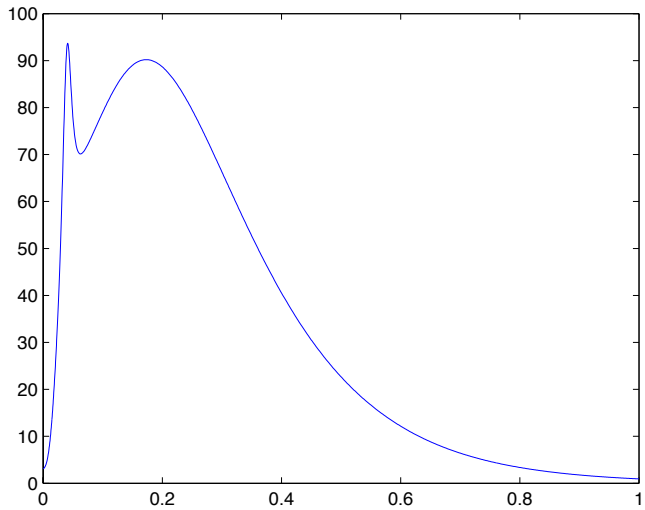

Figura 5.2: Normalised standard Adolf Rengel distribution without delta. The delta peak introduced for the simulations appear at point 0.18 and 0.36

5.2.4 the recoherence and the fundamental role of non-equilibrium vibrational structure

The phonon antenna mechanism is at the basis of the fundamental role of the reborn of coherence inside the quantum local site of our system. Locally the system taking advantage of non equilibrium quantum properties in the pico second time scale when the presence of a structured environment produce peaked value for the phonon energies which are resonant (approximately of the same value) with the difference in energy of two exciton (in the case of the dimer, the only two present).

As we can see the presence of the noisy environment does not destroy totally the coherence into the system, but the sharp resonant peak permits the continuous regeneration of that coherence into the sites population for a very longer time. Both values more or less asimptotically verge at the same plateau value for very long time of the state evolution,as expected. The plateau limit is a consequence of the presence of the phonon both into with the local systems are inserted.

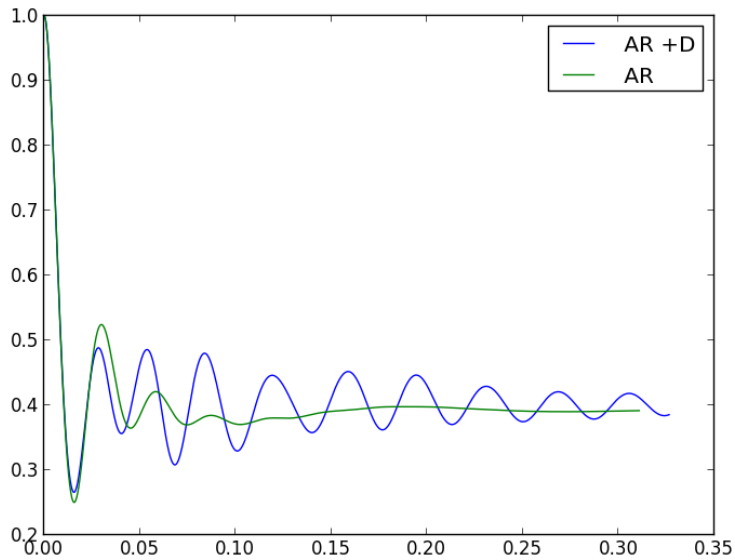

Figura 5.3: Population in the dimer site 1 obtained with a standard Adolf-Rengel distribution and with a standard with delta peak in $180cm{-}1$

5.2.5 the coupling with the environment

The environment plays a fundamental role into these type of system, so another useful quantities of relevance is the strength coupling between the system and the environmnt. As we can easily expect variation into this value produce great variation into the dynamics of the system.The presence of the resonant peak will always support the reborn of the coherence in a way or another,but because of the different value of the value of the coupling with the environment, the population dynamics will move from a more dumped one or to toward a more isolated dumped Raby-like system that show an oscillatory behave (see the oscillatory term into equation (4))

As we can see from figure 5.4 the presence of delta always substains the reborn of coherences inside the system, but the coupling with the environment greatly modify the dynamics. A strong coupling with the bath produce, as expected, a strong dumping that appears in a double exponential decay and second a plateau in the value of population lower, while a weaker coupling first of all induce an higher

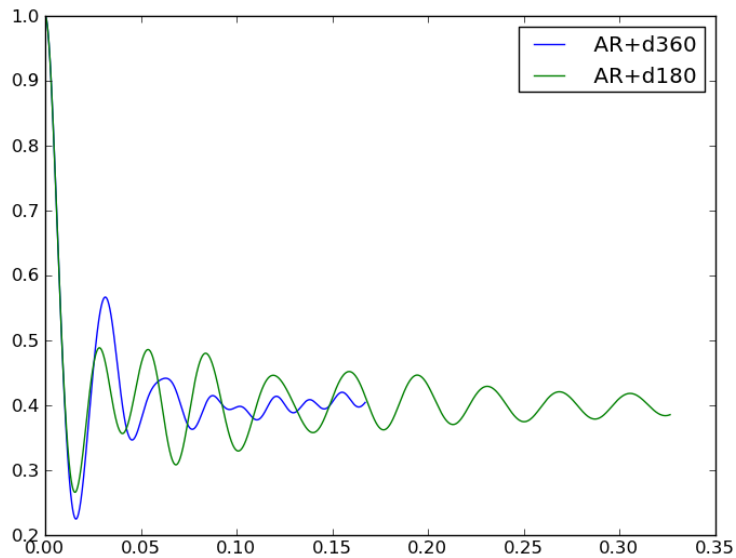

Figura 5.4: Population in the dimer site 1 obtained with an Adolf-Rengel with a delta peak on $180cm^{-1}$ and $360cm^{-1}$

value of the population asymptotic limit and a softer decay of the population, and moreover a net oscillating term.

5.2.6 Additional random noise

In order to take in account other additional random effects above which average (e.g. see the optical spectra formula) we can add some static randomness inside our system modifying our initial site value of energy. We start with this hypothesis: being that a general mode of the molecula it's always in the range of $10^{13}, 10^{14}$ seconds,each of this mode can be considered static respect the energy transfer, which moves in the picosecond timescale, so it will produce a static variation into the excited energy level of each site. Here a first result with the presence of the resonant mode and without

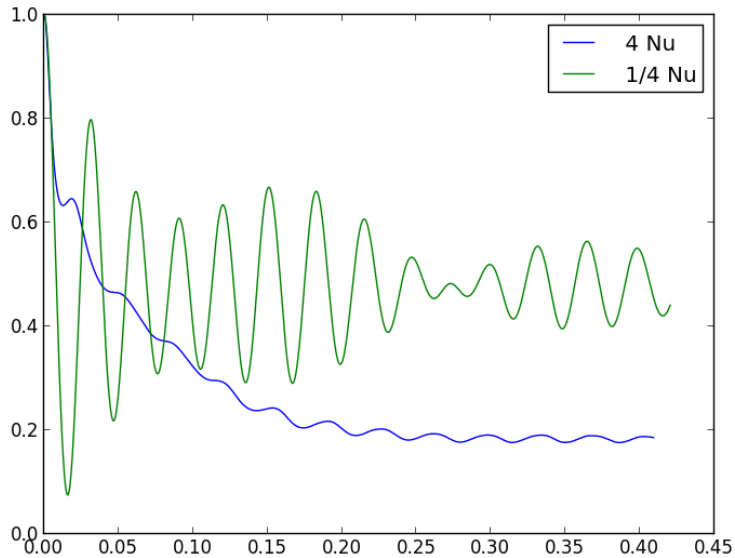

Figura 5.5: Different dynamics resulting from different strength coupling with the environment

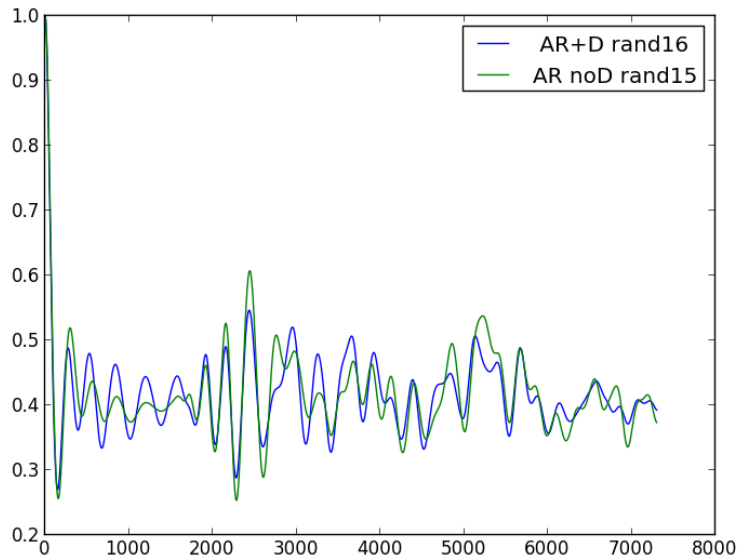

Figura 5.6: Averaged simulation for populations for the Adolf Rengel distribution with a settings value of the Smith cut-off Chi=20 and for each chain of 200 sites

The graph shows some features:

1. in the first picosecond the behave it's quite similar to a non random population (see fig(5.1))

2. a sudden high amplitude reborn of population which is very similar both for the spectral distribution with resonant and no resonant mode.

3. After around $0.25\times10-3$ picosecond we have a loss in the structure of the coherence;to be sure this qeffect arise from the introduction of randomness into the system we first have to take in account the accumulation of error inside our simulation,the lost of the norm of the state at a certain runaway time (see paragraph2.6.2 and fig 2.5) caused by a insufficient Schmidt truncation; in other word in order to investigate properly a random normal effects to compare with some experimental spectra first of all we must produce a more detailed simulation.

(a)

Higher energie antennacm^{-1}	lower energie antenna cm^{-1}
1051.2219117333091	993.5408611683903
1062.7355617394030	995.6801148476144
1050.6039684374250	1000.040518614079
1057.9278694405500	1004.4171138793954
1047.2970555313029	1003.432906300135
1052.2562514848751	1010.7741960189685
1065.2139014795459	996.9832360422838
1051.005637134137	994.6951834486741

(b)

Higher energie antenna cm^{-1}	lower energie antenna cm^{-1}
1053.2913431155830	998.6862714451294
1052.6506925406741	1001.569531780249
1029.3402825750420	1002.7196623122578
1037.1049564797320	1009.1629190416658
1059.4935570340319	1005.6390848901821
1052.8911763378601	1001.8801763736036
1062.8445222092330	993.93108508055831

Then we have refined our simulation in a more proper way,using a standard set of random number for both the spectral distribution and rising the numerical precision setting the value of the Schmidt cut-off Chi=38 to be sure to avoid the runaway time effects,and in order to take also in account border effects,a value of a total chain length of 480 sites (normal mode). Here the set of random number putted into the energy sites parameter for each simulation

and the new populations graph (5.7) which shows how the artifact effects disappear after the correction.

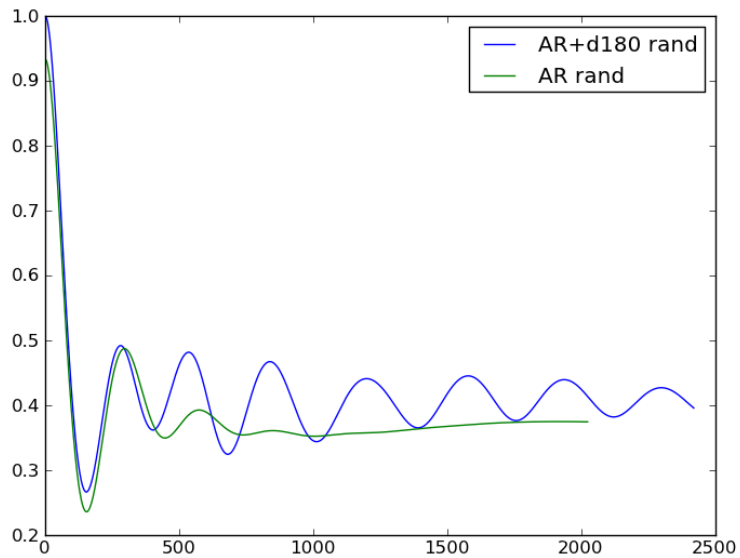

Figura 5.7: Averaged simulation for populations for the Adolf Rengel distribution with a settings value of the Smith cut-off Chi=38 and for each chain of 240 sites

5.2.7 Entanglement Measure: Von Newman entropy

The TEBD techniques possesses another powerful advantage which is the possibility to produce during our temporal evolution a direct, full, dynamical landscape of the terms of the total Schmidt decomposition of the state that derive from the application of the SVD for each time evolution on the total state; in this way we are able to obtain a direct measure of the two-blocks(subsystems) Von Newman entropy evaluated in each inter-site value (as stated in chapter 1 the tensor into which the λ are putted it's the matrix of basis transformation from one local site of the chain to another).

AS we can infer from image the difference in Entanglement production in the two time step consider,it's quite a few but present. Of a certain relevance is the presence of a peak in fig(5.6,5.7) in the inter-site near the central part of the chain, more precisely where lay the (protein antenna) system, .Despite we may expect this peaks follows from the contribute of the presence of the delta into the distribution

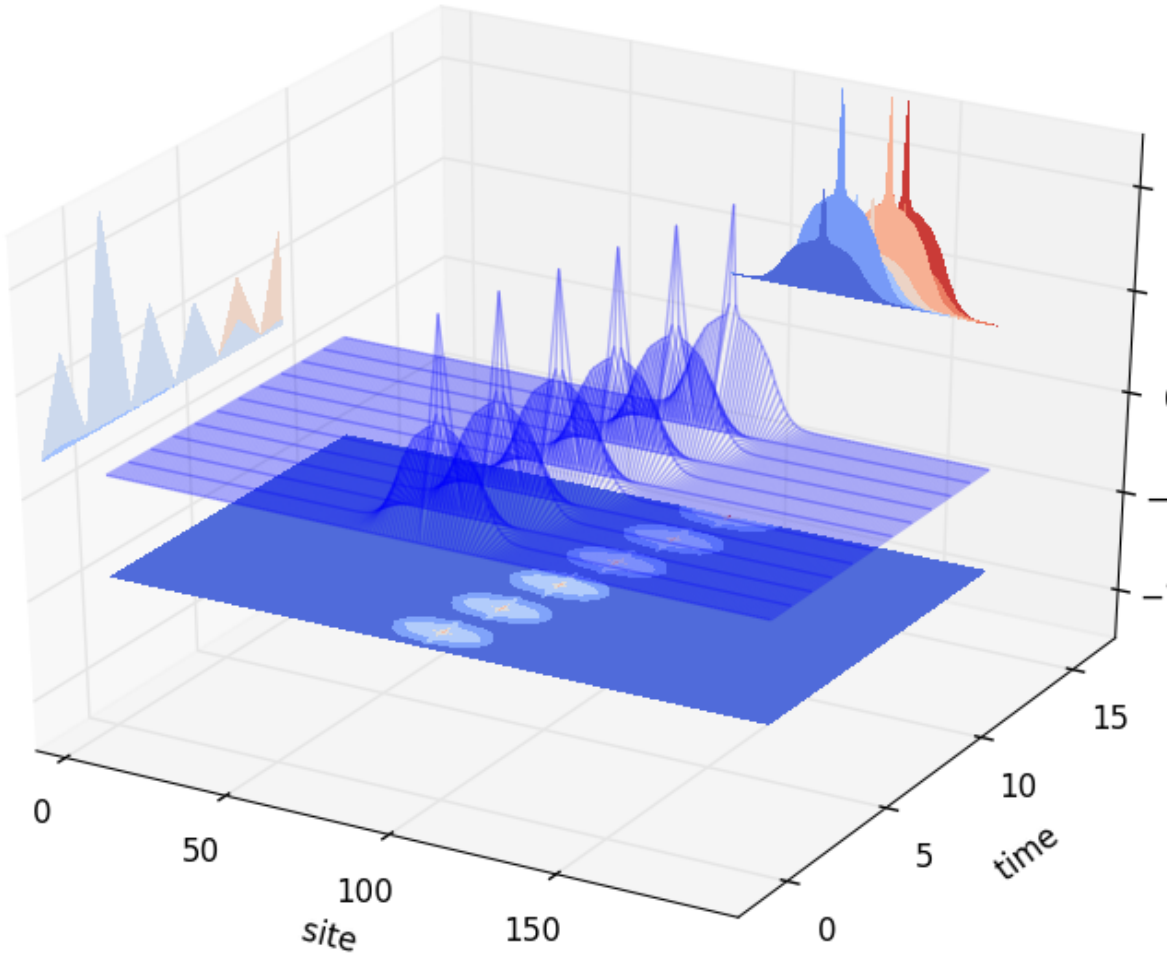

Figura 5.8: Adolf-Rengel spectral distribution + delta 180 cm^{-1} Von Newmann Entorpy graph for a timestep of 2000-2024

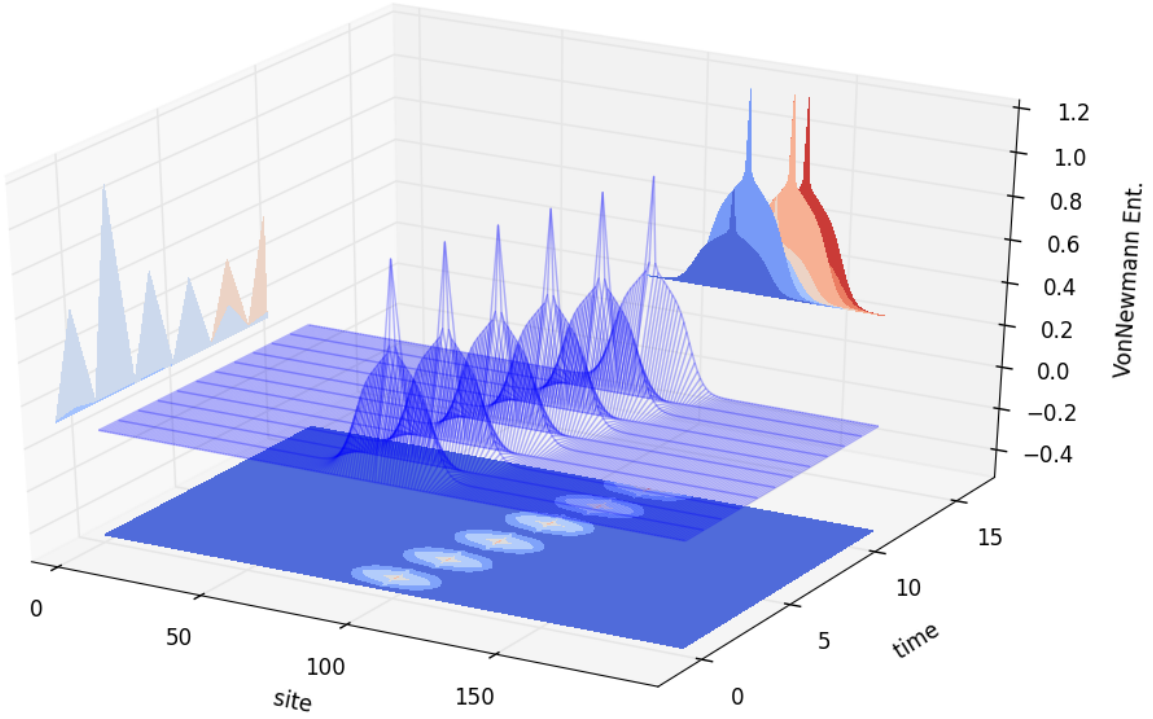

Figura 5.9: Standard Adolf-Rengel Von Newmann Entorpy graph for a timestep of 2000-2024

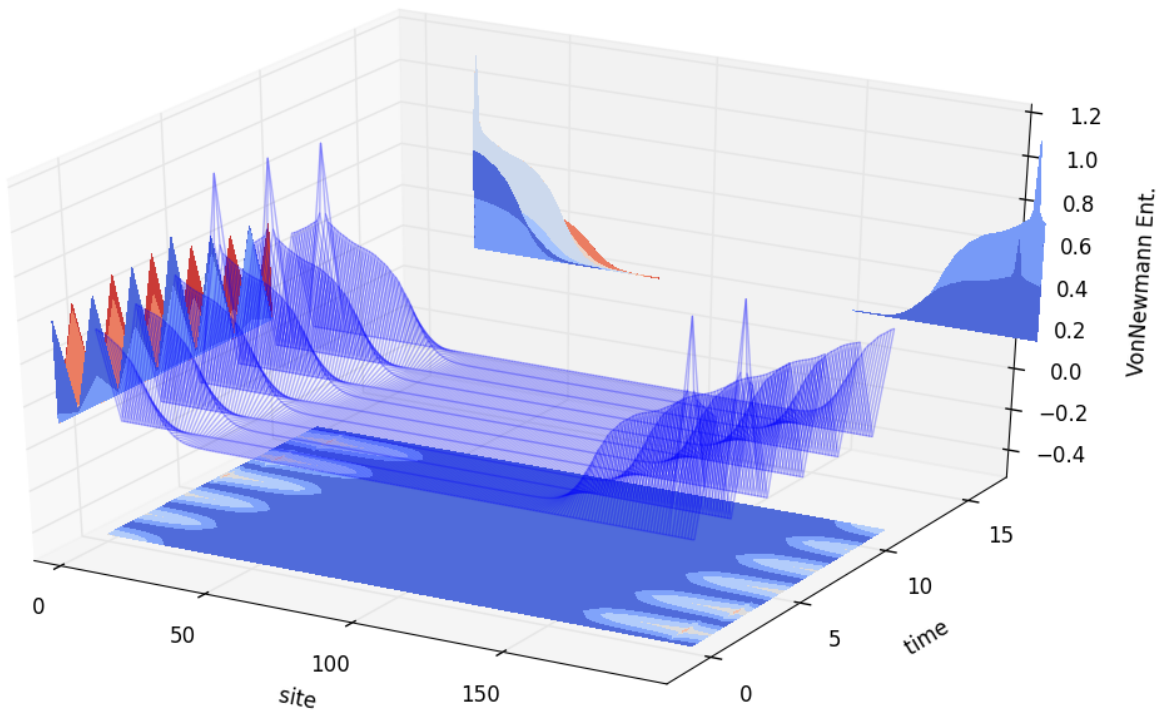

Figura 5.10: Adolf-Rengle + delta 180 cm^{-1} Von Newmann Entorpy graph for a timestep of 4000-4024

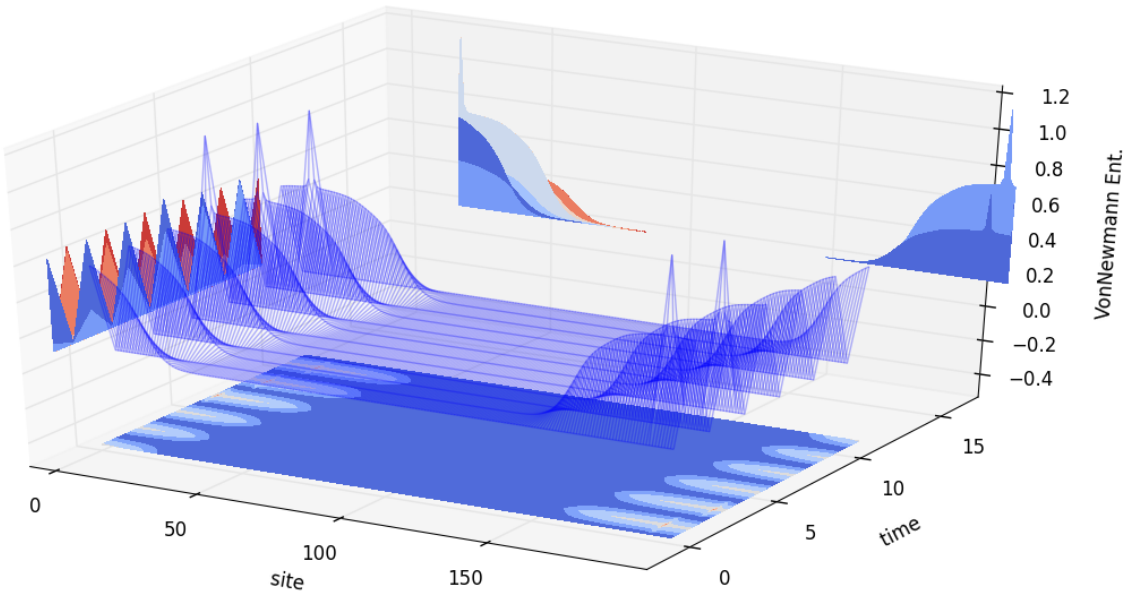

Figura 5.11: Standard Adolf-Rengel Von Newmann Entorpy graph for a timestep of 4000-4024

at a first glance the even seems to be very similar if not identical; despite of this in fig(4.10) we can see a little difference between the two distribution in the flux of Entropy between the environment modes,but not so showy. This may sound a bit unexpected, but taking a better look the the spectral distribution of the two Adolf-Rengel above considered, we can see that the role for the delta in terms of Entanglement production it's quite irilevant in this position,may be because of the presence of a phonon background that overlaps the delta peak contribute a lot.

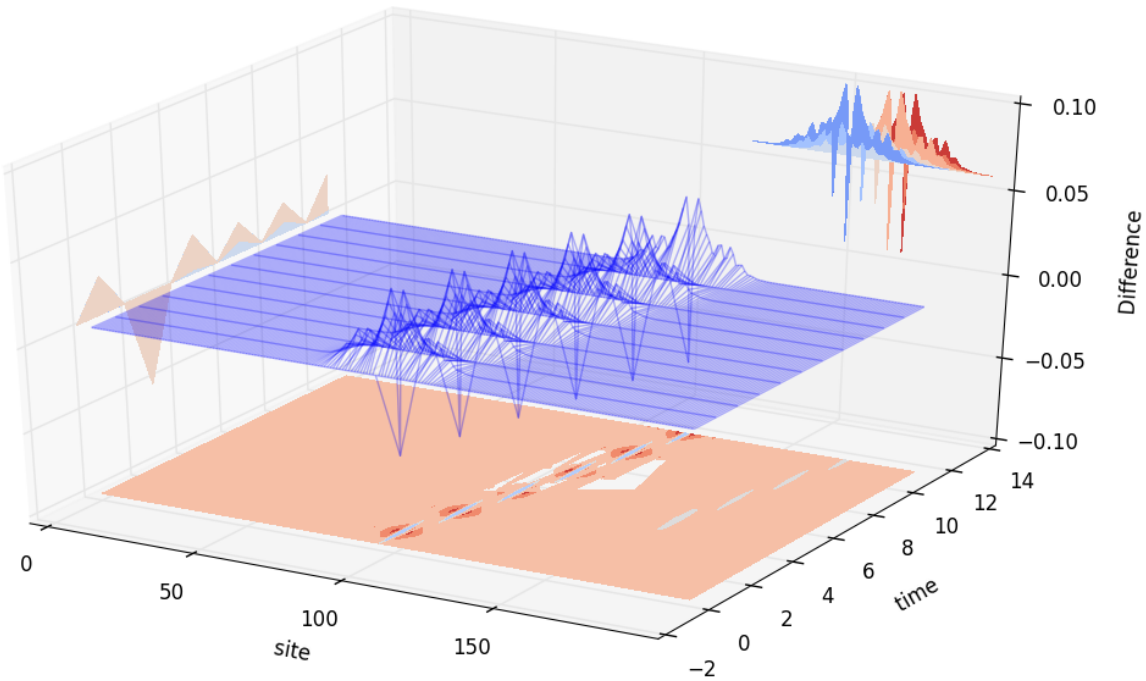

Figura 5.12: Graphical difference between the Von Newmann Entropy obtained without the resonant peak and resonant peak at $180cm^{-1}$

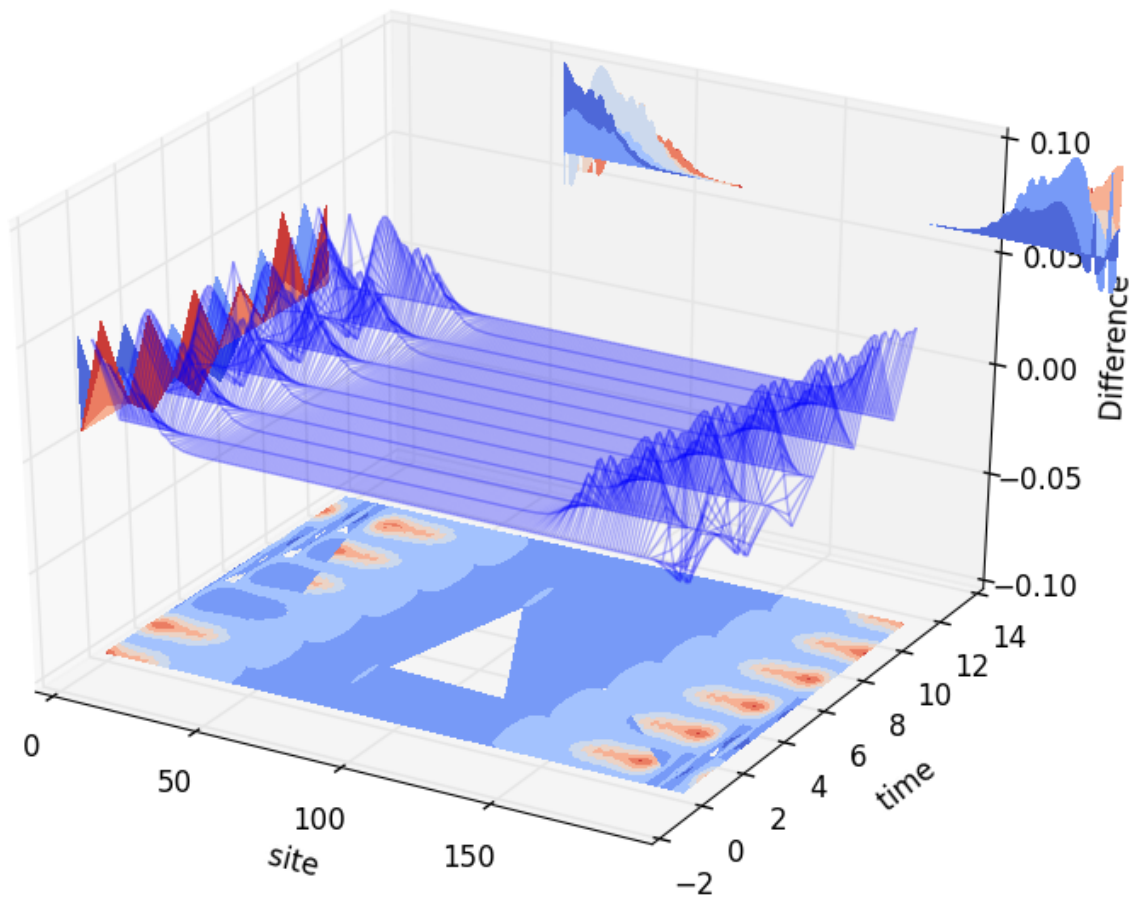

Figura 5.13: Graphical difference between the Von Newmann Entropy obtained in a timestep 4000-4024

5.2.8 The Double Environment

Thank to the agility of TEBD algorithm supported by the Orthopol algorithm, we can build simulation adding to each system (our protein antenna of the dimer in our case)a different chain projection (into the normal mode of the interaction hamiltonian) ,in other word a different spectra distribution which means to couple to each system an environment with different structural properties. This is another (important) step forward into the simulation of more realistic biological system , o more complicated system of every type,in general. Here the population graph for one site of the dimer

And the Von Newmann Entropy dynamics for two time step (1000,1024),(2000,2024)

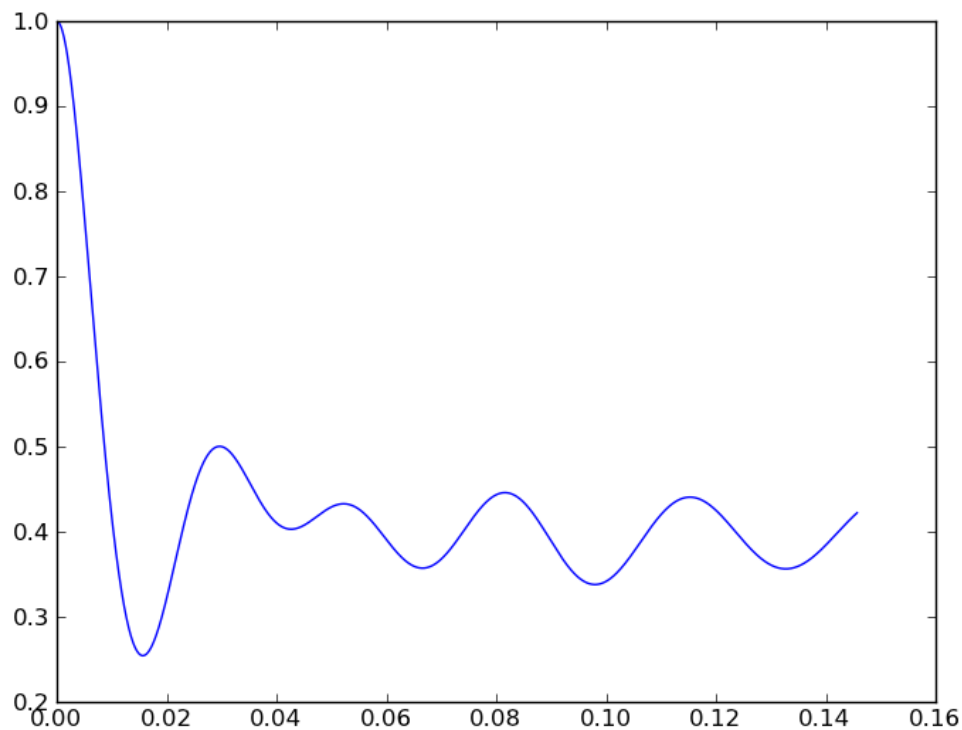

Figura 5.14: population of site 1 with a dimer coupled to two different structured environment

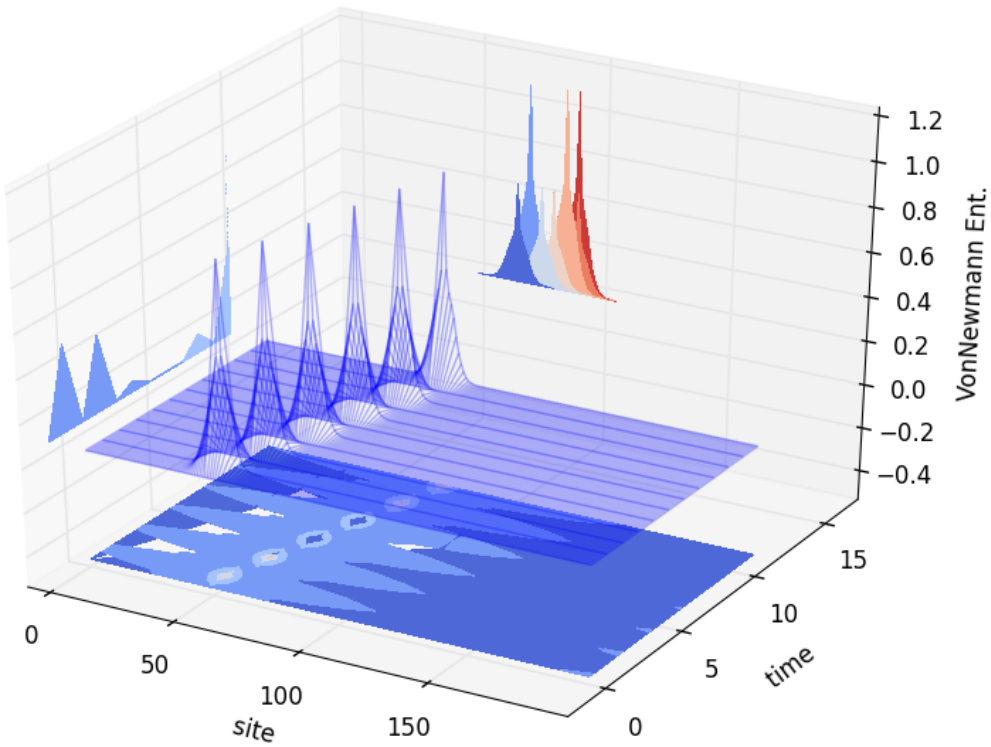

Figura 5.15: population of site 1 with a dimer couplde to two different structured environment

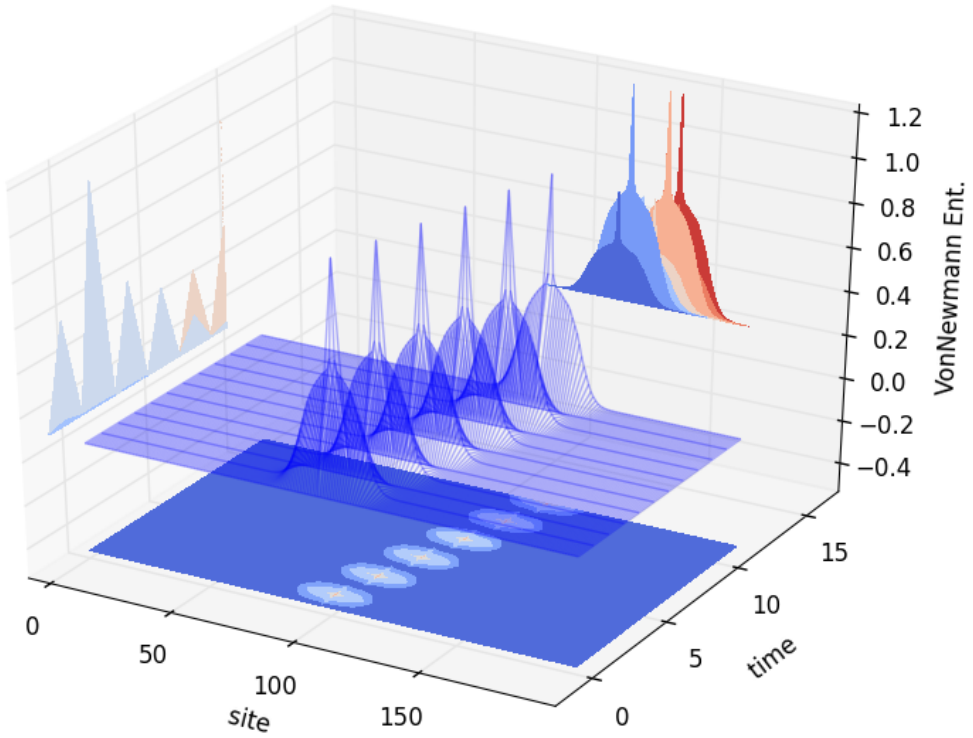

Figura 5.16: population of site 1 with a dimer couplde to two different structured environment

As we can see the presence of two different environment produce another dynamics more, into the flux of entanglement along the chain. The population dynamics shows the maintenance of the persistent oscillation due to the phonon antenna effect, even if only one environment site contributes to it. This shows a certain robustness of this phenomenology whereas a quantum system can take advantage of it. On the other hand the entanglement (Von newmann entropy) present a very peculiar behavior showing a non diffusive behavior.

Capitolo 6

Conclusion

The aim of this thesis. First the presentation of the numerical outcome concerning the local population dynamics of the excitons inside the antenna sites of our dimeric system via our TEBD algorithm, at the light of the paradigms of the quantum biology above exposed. Thank to the principles of the noisy assisted transport, an intermediate degree of environmental noise which, as demonstrated into quantum network simulation, sustains the flux along a general transport chain , and the phonon antenna principle, which explains how the system take advantage of some specific long lived environmental vibrational modes, is possible shed light into the deeper mechanism of how a coherent transport of energy along the chain of an excitonic system (a chain composed of two level systems of protein in excited state which produce site Frenkel excitons). As shown in fig 5.5 the coupling strenght with the environment produce a great variation into the dynamic of the local population, so only an intermediate level of noise is permitted in order to obtain performant dynamics; higher level of noisy will produced an unavoidable quantity of dephasing that will suppress the coherence while on the other hand a too low level of noise will give raise to a stronger effect of localization (Anderson effect) which will obstruct the transport dynamics Alongside with this principle, as is evident in fig 5.3, the phonon antenna principle that lasts for time of the order of the picosecond; a time scale which permit to the transport chain the transport of energy without losses.

Second aim was an overview of the technique, it's methods , and its potential in

order to present its agility in showing some global features like the Von Newmann and how modifications to the structure of the objects modeled can be easily handled with the numerical tool of the TEBD. Thank to the ORTHOPOL algorithm that makes use of the orthonormal polynomials we can map an open system of the type of continuous spin-boson model into a (theoretically) semi infinite chain of normal modes. Being the spectral function the description of the overall strength of the interaction of the system with the reservoir modes of frequency ω we can produce the new energy parameters for the chain, and the associated hopping parameters of the 1-D projected chain, in order to simulate in the TEBD code the system-environment interaction. This straightforward technique shows the potential of a full non-equilibrium, non-perturbative, non-Markovian (inhomogeneous chain) description of the system-environment dynamics. The agility of the TEBD technique also permit us the visualization of global information as the von Newmann entropy of the 1-D chain for every time step.It is even possible easily inserting static local random effect or modification in the conformational structure of our dimer, that from an informational point of view means the contemporary use of different environmental spectras. This agility makes straightforward simulation of more and more complicated structures, far beyond a simple dimeric structure. This will be another very useful trait in the future for the modeling of more structured and reach protein complexes as the FMO and others even more complicated as the Photosystem II light harvesting systems.

Bibliografia

[1] M. Mohseni, Y. Omar, G.S. Engel, and M.B. Plenio (eds.), Quantum effects in biology, Cambridge Univer- sity Press, Cambridge 2013.

[2] Proceedings of the 22nd Solvay Conference in Chem- istry on "Quantum Effects in Chemistry and Biology, Procedia Chemistry 3 (2011).

[3] L. Hartmann, W. Du?r and H.J. Briegel, Steady state en- tanglement in open and noisy quantum systems at high temperature, Phys. Rev. A 74 (2006), 052304.

[4] Blankenship, R. Molecular Mechanisms of Photosynthesis (Wiley-Blackwell, 2002)

[5] Van Amerongen, H., Valkunas, L. & van Grondelle, R. Photosynthetic Excitons (World Scientific, 2000)

[6] Matsuzaki, S., Zazubovich, V., Rätsep, M., Hayes, J. & Small, G. Energy transfer kinetics and low energy vibrational structure of the three lowest energy Qy-states of the Fenna-Matthews-Olson antenna complex. J. Phys. Chem. B 104, 9564–9572 (2000).

[7] R. P. Feynman, Opt. News 11, 11 (1985): Found. Phys. 16 507 (1986); Int. J. Theor. Phys. 21, 467 (1982).

[8] G. Vidal, Phys. Rev. Lett. 98, 070201 (2007)

[9] G. Vidal, Phys. Rev. Lett. 93, 040502 (2004)

[10] Engineering Coherence Among Excited States in Synthetic Heterodimer Systems

[11] E. Collini, C. Wong, K. Wilk, P. Curmi, P. Brumer, and G. Scholes, Coherently wired light-harvesting in photo- synthetic marine algae at ambient temperature, Nature 463 (2010), pp. 644 - 649.

[12] S.F. Huelga, A. Rivas, and M.B. Plenio, Non- Markovianity assisted Steady State Entanglement, Phys. Rev. Lett. 108 (2012), 160402.

[13] On the relation of protein dynamics and exciton relaxation in pigment-protein complexes: an estimation of the spectral density and a theory for the calculation of optical spectra